International Journal of Greenhouse Gas Control 130 (2023) 103991

Contents lists available at ScienceDirect

International Journal of Greenhouse Gas Control

journal homepage: www.elsevier.com/locate/ijggc

SEWGS integration in a direct reduction steelmaking process for CO_2 mitigation

Nicola Zecca [a,*], Paul D. Cobden [b], Leonie Lücking [c], Giampaolo Manzolini [a]

[a] Politecnico di Milano, Dipartimento di Energia, via Lambruschini 4, 20126, Milano, Italy
[b] Swerim AB, Aronstorpsvägen 1, 974 37 Luleå, Sweden
[c] TNO, Westerduinweg 3, 1755 LE, Petten, the Netherlands

ARTICLE INFO

Keywords:
Steel
DRI-EAF
BF-BOF
SEWGS
CCS
GHG
CO_2 mitigation

ABSTRACT

The iron and steel industry represents one of the most carbon intensive sectors accounting for roughly 25% of CO_2 emissions generated by the industrial sectors and for 7% of total energy sector emissions. The aim of this work is to assess the techno-economic analysis of the integration of the SEWGS technology in the DRI-EAF process to reduce the carbon footprint of this steelmaking route. The study has been carried out using plant data taken from literature and investigating possibilities of GHG mitigation by introducing carbon-capture technologies such as MEA and MDEA scrubbing or the SEWGS technology. The latter solution shows environmental and economic advantages compared to the cases based on amine scrubbing. A reduction of CO_2 emissions close to 90%, with respect to the BF-BOF route, can be achieved with the implementation of the SEWGS when a renewable electricity scenario is considered. Economic KPIs such as the Levelised Cost of Hot Rolled Coil and the Cost of CO_2 avoided have been computed for all the plants. In addition, a sensitivity analysis on natural gas and electricity prices has been carried out. The integration of the SEWGS technology represents a promising solution for the reduction of the carbon footprint of the DRI-EAF process and, potentially, it could be commercially viable in the near future considering that the DRI and EAF processes are already globally commercialised.

1. Introduction

In the pathway towards an economy with net zero GHG emissions, the decarbonization of the industrial sector represents one of the main challenges for the next decades. The steelmaking industry is one of the most energy and carbon intensive relying on the use of fossil fuels. Indeed, in 2019 the iron and steel sector globally accounted for 845 Mtoe[1] of energy consumption, representing 20% of industrial energy use and 8% of total final energy use (International Energy Agency, 2020). In addition, the steel sector, in the same period, accounted for 2.6 Gt of direct carbon dioxide emissions, representing roughly 25% of CO_2 emissions generated by all the industrial sectors and 7% of total energy sector emissions (International Energy Agency, 2020). Different routes can be used to produce steel. More than 80% of steel is globally produced via primary routes from iron ore and some scrap while the rest is manufactured via recycled scrap. The blast-furnace and basic-oxygen-furnace route (BF-BOF) represents 70% of global steel production and around 90% of primary production (International Energy Agency, 2020). The remaining 10% of primary reduction is accounted for by the direct reduced iron route (DRI) (International Energy Agency, 2020). BF-BOF and EAF (DRI-EAF and scrap-based EAF) routes represent the 95% of total steel produced (International Energy Agency, 2020). Considering these data, the decarbonisation of the steelmaking sector becomes crucial.

In this paper the techno-economic assessment of the integration of the Sorption Enhanced Water Gas Shift (SEWGS) technology in the production of direct reduced iron is performed. The integration of the SEWGS allows the removal of carbon dioxide from the gas stream that leaves the top of the shaft furnace. In the shaft furnace iron ore is reduced by carbon monoxide and hydrogen that are produced via methane reforming, generating direct reduced iron at the bottom of the shaft. In addition to the CO_2 stream that can be compressed and stored, the SEWGS also produces a H_2-rich stream that can be used as fuel in the reformer thus generating CO_2-free flue gases. The integration of the SEWGS in the DR process has therefore the strong potential to reduce the carbon emissions of this process.

* Corresponding author.
E-mail address: nicola.zecca@polimi.it (N. Zecca).

[1] Mega ton of oil equivalent

https://doi.org/10.1016/j.ijggc.2023.103991
Received 21 June 2023; Received in revised form 8 September 2023; Accepted 30 September 2023
Available online 27 October 2023

Nomenclature

Acronyms

BF	Blast furnace
BOF	Basic oxygen furnace
CA	CO_2 Avoidance [%]
CCA	Cost of CO_2 avoided [€/t_{CO2}]
CCR	CO_2 Capture Ratio [%]
CCS	Carbon Capture and Storage
CI	Carbon Intensity [$t_{CO2}/t_{product}$]
Co	Contingencies [€]
DR	Direct reduction
DRI	Direct reduced iron
DRP	Direct reduction process
EAF	Electric arc furnace
EPC	Engineering, Procurement and Construction [€]
FCR	Fixed Charge Rate [%]
GHG	Greenhouse Gases
HM	Hot Metal
HRC	Hot Rolled Coil

Symbols

C_f	Fixed Costs [M€/y]
C_v	Variable Costs [M€/y]
η	Efficiency [-]
τ	Plant availability [-]
r	Interest rate [%]
T	Plant lifetime [years]
LCOHRC	Levelised Cost of HRC [€/t_{HRC}]
LS	Liquid Steel
MDEA	Methyldiethanolamine
MEA	Monoethanolamine
NG	Natural gas
NGCC	Natural Gas Combined Cycle
OC	Owner's Cost [€]
PEC	Primary Energy Consumption [GJ/$t_{product}$]
SEWGS	Sorption Enhanced Water Gas Shift
SPECCA	Specific PEC for CO_2 Avoided [GJ/t_{CO2}]
TAC	Total Annualised Cost [M€/y]
TDPC	Total Direct Plant Cost [€]
TEC	Total Equipment Cost [€]
TIC	Total Installation Cost [€]
TPC	Total Plant Cost [€]
WGS	Water gas shift

Subscripts

e	Electric
h	Hydraulic
m	Mechanical
p	Polytropic

1.1. The DRI-EAF process

The DRI-EAF process represents an alternative primary steel production route to the traditional BF-BOF route (International Energy Agency, 2020). Solid primary iron (DRI) is produced from iron ores through reducing gases in special furnaces. The reducing gases are mainly produced from natural gas or coal. The DRI is then melted in electric arc furnaces to produce steel. Different processes have been developed which mainly differentiate based on the type of furnace adopted. Between all the commercial available DRI processes, the Midrex represents the one with the largest market share, equal to the 60% in the 2020 (World direct reduction statistics, 2020). For this reason, this process has been selected and investigated in this work.

The performances of the DRI-EAF plants are well known as this process has been commercially available for decades. (Cavaliere, 2019) shows a consumption of the Midrex plants ranging between 258 and 270 m^3/t_{DRI} of natural gas and 90–135 kWh/t_{DRI} of electricity, leading to a total primary energy consumption of 10.3–10.9 GJ/t_{DRI}. Regarding the CO_2 emissions, 1.269 t_{CO2}/t_{steel} are generated, resulting as the sum of "upstream", "process" and "EAF" emissions, respectively equal to 0.244, 0.638 and 0.388 t_{CO2}/t_{steel} (Cavaliere, 2019). When the whole DRI-EAF process is considered, an energy consumption of 18.54 GJ/t_{steel} is indicated by (Cavaliere, 2019), where the 11.58 GJ/t_{steel} of the "process" represents the main contribution, at which the "upstream" (2.58 GJ/t_{steel}) and the "EAF-power" (4.11 GJ/t_{steel}) are added.

Many models of the shaft furnace, the core of the direct reduction process have been developed. In (Lu et al., 2019) the competitive adsorption behaviour of CO and H_2 molecules on FeO surface is investigated by thermogravimetry and molecular dynamics simulation. The model, based on Langmuir adsorption equations, shows that the CO adsorption is influenced by oxygen and iron molecules while the H_2 adsorption is governed only by oxygen. (Rahimi and Niksiar, 2013) developed a model for moving-bed reactors, adopting a grain model and considering the reduction of Fe_2O_3 by a gas mixture of CO and H_2. The model is compared to experimental data, showing an average error of 1.2%. Also (Palacios et al., 2015) studied numerically and experimentally the iron ore reduction by a gaseous mixture of H_2 and CO. A fixed-bed reactor was designed to perform the test and a mathematical model of the reduction reactions was developed. Furthermore, the mathematical model of a direct reduction moving bed reactor for the production of sponge iron, adopting a grain model is shown in (Nouri et al., 2011). The model shows a good agreement with the data of Foolad Mobarake plant (Isfahan, Iran). A mixture of CO, H_2, CO_2, H_2O, N_2 and CH_4 is considered as reducing agent. A gas mixture constituted by those components is also considered by (Alamsari et al., 2010, 2011; Hamadeh et al., 2018; Shams and Moazeni, 2015). (Shams and Moazeni, 2015) developed a model that simulates the reduction, transition and cooling zones of a Midrex shaft furnace, comparing the model with real plant data. (Alamsari et al., 2010) used a finite element method (FEM) to solve the mathematical model of a sponge iron reactor. (Hamadeh et al., 2018) simulated the reduction of iron ores using the REDUCTOR model where equations are solved by applying finite volume technique. The results are compared to plant data. The REDUCTOR model was developed by (Ranzani da Costa et al., 2013). The axisymmetric steady-state 2D model of a counter-current moving bed reactor was used to simulate the reduction of iron ores by pure hydrogen, showing the potentiality, in terms of reduction of CO_2 emissions with respect the conventional DR process. A CFD simulation of a Midrex shaft furnace is also investigated in (Zare Ghadi et al., 2017), where H_2 is used as reducing agent and one and two gas intake ports are simulated.

On the other hand, fewer studies that include the whole direct reduction process are available. The complex interactions between the reformer and reduction furnace in a Midrex plant were investigated by (Alhumaizi et al., 2012), where a first principle models for the reformer and the reduction furnace, in addition to models for auxiliary units such as heat recuperator, scrubber and compressor were developed. The effects of key input parameters (such as the recycle ratio, the scrubber exit temperature, the flow rate of injected oxygen, the flow rate of natural gas added after the reformer, to the transition zone, to the reformer and to the cooling zone) on the performance of the plant were studied. (Béchara et al., 2018) adapted the results of the REDUCTOR model of the shaft furnace to simulate a whole DR process in Aspen Plus, comparing the results with data of two different Midrex plants and optimising the performance of the process by varying some of the

process parameters. A natural gas (NG) based Midrex shaft model has been developed by (Sarkar et al., 2018) and validated for emission and energy estimation for crude steel production. The model is used to investigate the possibility to use instead of natural gas other H_2-rich fuels, namely the Coke Oven Gas (COG) and syngas from coal gasification. The results are then compared to the performance of the BF-BOF route. The NG based DR process was also developed by (Rechberger et al., 2020) as a first step to assess the possibilities of injecting hydrogen, transitioning to H_2-based DR process. The study shows that the emissions of the hydrogen-based process strongly depends on the carbon footprint of electricity used to produce the H_2 and that the process emits less CO_2 than the NG-based DR process when the electricity carbon footprint is less than 120 kg/MWh.

1.2. Objective of the work

The aim of this work is to assess the techno-economic analysis of the integration of carbon capture technologies in the Midrex direct reduction process to decrease the carbon footprint of this steel production route. The analysis was carried out simulating different plants configurations, a conventional DRI-EAF plant based on Midrex technology, a Midrex plant with a post-combustion MEA carbon capture section, a Midrex plant with a pre-combustion MDEA carbon capture section and a Midrex plant with a pre-combustion SEWGS carbon capture section. The performances of an electric arc furnace and of a rolling section are also taken into account, in order to evaluate the performances of the whole steel production process. The results are then compared to a reference DRI-EAF plant and to a reference BF-BOF plant.

In this study, public available data of an operating Midrex plant have been used. Nevertheless, there exist DRI plants that use less amounts of natural gas and more hydrogen (i.e. through electrolysis) going to the shaft furnace that would potentially give some advantages or disadvantages with respect to the plants considered in this work. In addition, the abatement of direct emissions from the electric arc furnace have not been addressed in this paper. It is also recognized that other approaches, such as the use of green hydrogen could lead to a further reduction of the CO_2 emissions.

2. Investigated plant configurations

2.1. Base DRI-EAF plant

In a conventional DRI-EAF plant, natural gas is used as feedstock for the production of the reducing gas (Fig. 1). Natural gas is first mixed with the recycled top-gas exiting the shaft furnace. The mixture is then heated exploiting the waste heat of the flue gas from the reformer. Subsequently it is fed to the reformer to produce the reducing gas, mainly H_2 and CO, necessary for the reduction of iron ores. In the furnace, the oxygen present in the iron ores, composed mainly of haematite (Fe_2O_3), is removed. The direct reduced iron exits the bottom of the shaft furnace and it is sent to an electric arc furnace to be melted and produce steel.

The top-gas exiting the furnace is cooled in a scrubber. Downstream the scrubber the top-gas is divided into two streams; the one used as fuel for the reformer is roughly 33% of the total, while the remaining part is recycled back and mixed with fresh natural gas as described above. If necessary, some natural gas can be also used as fuel in the reformer. The whole process works at a pressure slightly above atmospheric. A compressor, due to the pressure drops in the system (mainly in the reformer and in the shaft furnace) is necessary to recycle part of the top-gas.

Two main emissions points can be identified: the flue gas of the reformer and the electric arc furnace. About the flue gases, emissions are related to the utilisation of the top-gas as fuel to supply the heat necessary to the reforming reaction. These gases contain relevant amounts of CO and CO_2. Furthermore, some additional natural gas may be provided to the reformer. As mentioned above, the other emission point is related to the electric arc furnace where the DRI is melted and further prepared for steel production. In any case, the main contribution to the emissions of the whole process is given by the flue gas of the reformer.

For this study the ArcelorMittal Montreal plant, located in Contrecœur (Quebec), Canada, was selected as base case since real plant data are available in literature (Béchara et al., 2018; Hamadeh et al., 2018). The data used in this work and reported in Table 1 are:

- the composition and temperature of the iron ores;
- the daily production of direct reduced iron (corresponding to 0.814 Mt_{HRC}/y);
- the mole flow, composition and temperature of the reducing gas entering the shaft furnace;
- the mole flow, composition, temperature and pressure of the top-gas exiting the shaft furnace.

2.2. DRI-EAF plant with post-combustion MEA carbon capture section

The first option considered to reduce the carbon footprint associated to the direct reduction process is the addition of a post-combustion MEA carbon capture section (Fig. 2). The flue gases from the reformer are sent to an absorber column where they are contacted with lean MEA. The CO_2 in the flue gas is absorbed by the solvent. The decarbonized flue gases leave the top of the absorber while the rich solvent is heated and

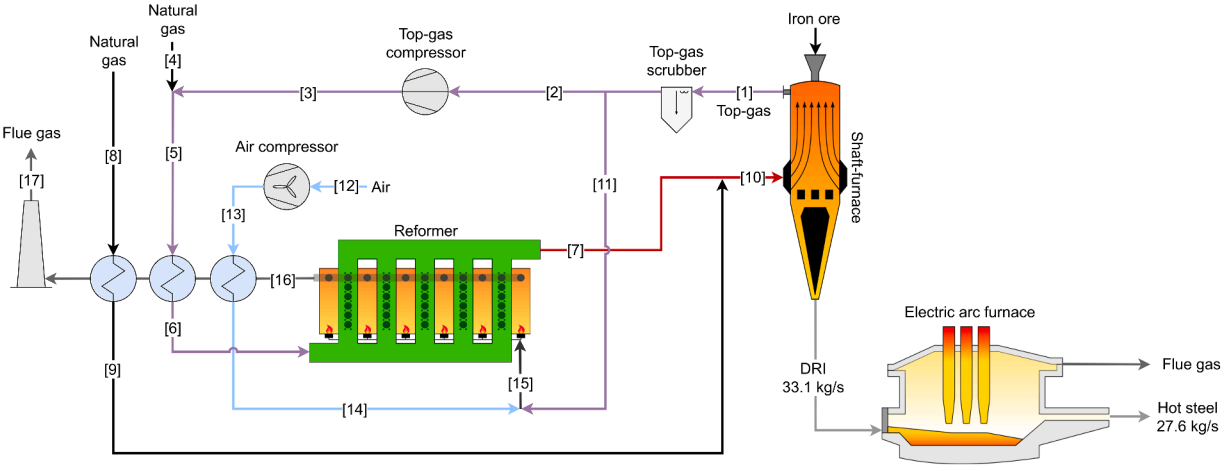

Fig. 1. Conventional Midrex plant plus electric arc furnace.

sent to the stripper column. A CO_2-rich stream leaves the top of the stripper while the regenerated solvent exits from the bottom. The high-purity CO_2 is compressed to 80 bar in a multistage compressor, liquefied by cooling to 25 °C and pumped to 110 bar. The carbon capture ratio is set to be 90% of the CO_2 present in the flue gases. Higher carbon capture ratio could be achieved but this implies a higher steam demand for the solvent regeneration. The steam necessary for the solvent regeneration can be in part produced exploiting the heat available in the top-gas of the shaft furnace or in the flue gases of the reformer. For simplicity of comparisons, the rest of the steam is assumed to be produced in a natural gas boiler. The flue gas from the boiler are not threated in the MEA carbon capture section but directly vented, contributing in this way to the emissions of the whole process (Fig. 2).

In this plant configuration no big modifications need to be implemented with respect to the original DRI-EAF plant. In fact, the main equipment, the shaft furnace and the reformer will work under the same conditions. Therefore, this solution could potentially be integrated into an existing plant.

2.3. DRI-EAF plant with pre-combustion MDEA carbon capture section

The second plant configuration, analysed in this work to reduce the emission of the DRI production process, considers the integration of a pre-combustion carbon capture process. The top-gas coming from the shaft furnace and normally used as fuel for the reformer contains a high quantity of CO and CO_2 (Table 1). The direct reduction process can be decarbonised by shifting the CO to CO_2 through the WGS reaction and then capture the CO_2 in a MDEA carbon capture section. The total conversion of CO into CO_2 equals 89% and it is achieved by means of three WGS reactors with an overall steam to CO ratio equal to 2.1 (Table 7). A split configuration is adopted, with only 37% of the total gas stream sent to the first WGS reactor to decrease the overall steam requirements (Jansen et al., 2015). The products of the first reactor are then mixed with the remaining top-gas and sent to the following in-series WGS reactors to complete the conversion (Fig. 6). Before being shifted, the top-gas is compressed to 8 bar in order to decrease the dimensions of the vessels and favour the CO_2 capture in the MDEA carbon capture section. The shifted gas is first cooled to a temperature suitable to produce part of the steam necessary for solvent regeneration and then it is further cooled to 40 °C removing the condensed water. In the absorber column, the syngas is in contact with the lean solvent (MDEA) that absorbs the carbon dioxide. A decarbonized clean fuel exits the top of the column while the CO_2-rich solvent exits from the bottom being subsequently sent to the stripping column to be regenerated. The high-purity CO_2 exits the stripper column at the top and the evaporated water is removed in a condenser. The CO_2-rich stream is then compressed up to 78 bar in a multistage compressor, liquefied by cooling to 25 °C and pumped to 110 bar. The carbon capture ratio of the MDEA unit is set to 96%. A higher carbon capture ratio than the MEA case is necessary since not all the CO is shifted into CO_2. This implies that the unshifted CO will be converted into CO_2 in the reformer furnace, contributing to the whole emissions of the process. The H_2-rich stream is then used as clean fuel in the reformer (Fig. 3). Steam production is necessary for both the water gas shift reaction and for solvent regeneration. The heat available in the top-gas and in the flue gas of the reformer is used to generate steam. Furthermore, in addition to the steam generated cooling the gas fed to MDEA section (as mentioned above), some steam is generated by exploiting the heat available in the stream exiting the second water gas shift reactor. Indeed, the heat exchanger placed between the second and the third WGS reactor allows the production of steam while controlling the inlet temperature of the third WGS reactor. Similarly to the previous case, the rest of the steam is assumed to be produced in a natural gas steam generator.

In contrast to the plant configuration described in Section 2.2, some important changes in the plant layout must be implemented. First, an additional compressor for the top-gas that is first shifted and then

Table 1
Specifications of reducing gas, top-gas, iron ores and DRI.

Stream	Temperature [°C]	Pressure [bar]	Mole flow rate [kmol/h]	Molar composition [%]					
				H_2	N_2	H_2O	CO	CO_2	CH_4
Reducing gas	957	n.a.	7841	49.66	1.76	4.28	32.71	2.40	9.08
Top-gas	285	1.42	8611	40.28	1.02	19.03	19.58	17.09	2.95

Stream	Temperature [°C]	Pressure [bar]	Mass flow rate [kg/s]	Mass composition [%]					
				Fe_2O_3	Fe_3O_4	FeO	Fe	C	Gangue
Iron ores	−10	1.013	45.54	96.65	0.00	0.00	0.00	0.00	3.35
DRI	n.a.	n.a.	33.1	0.00	0.00	7.47	85.72	2.00	4.71

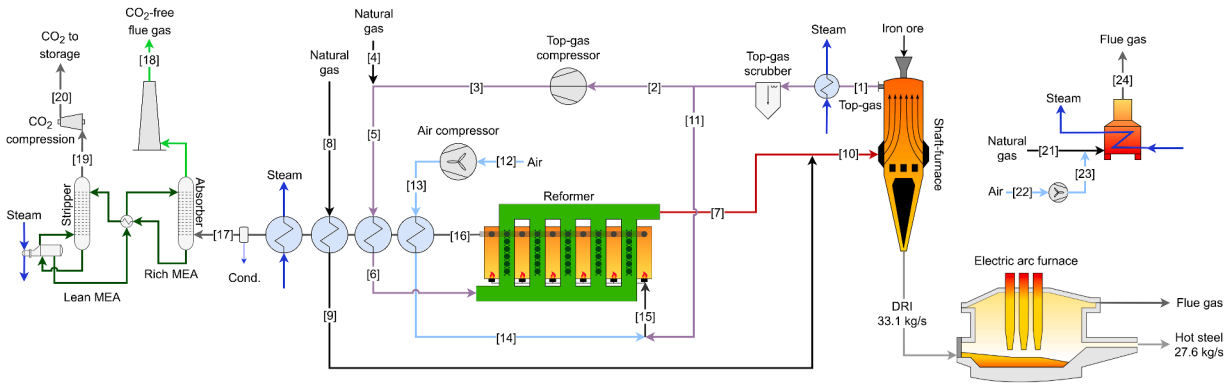

Fig. 2. Midrex plant with post-combustion carbon capture MEA section plus electric arc furnace.

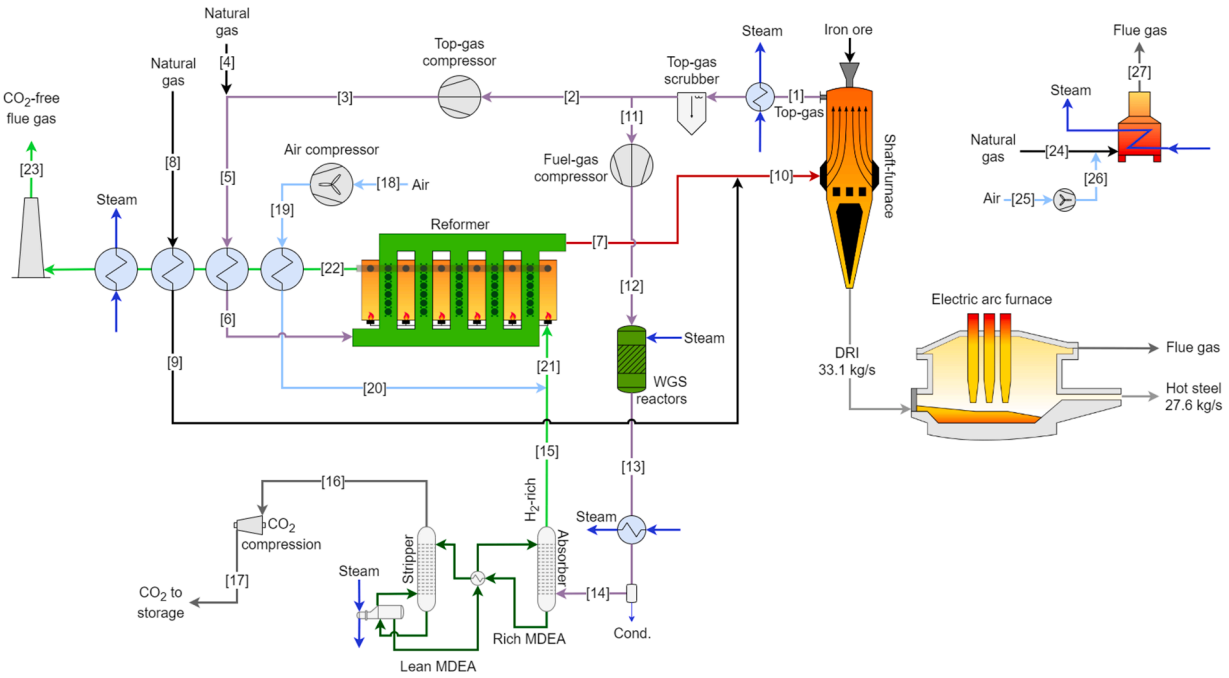

Fig. 3. Midrex plant with pre-combustion carbon capture MDEA section plus electric arc furnace.

decarbonised must be added. Secondly, the composition of the fuel used in the reformer is completely different from the fuel fed in the original configuration. This implies a different design of the reformer furnace. On the other hand, the shaft furnace does not change with respect to the original configuration since the same reducing gas is fed.

2.4. DRI-EAF plant with pre-combustion SEWGS carbon capture section

In the last option analysed for the decarbonisation of the DR process, a pre-combustion carbon capture section with the SEWGS technology is considered (Fig. 4). The layout of this plant configuration is quite similar to the one described in Section 2.3. The concept is the same, producing,

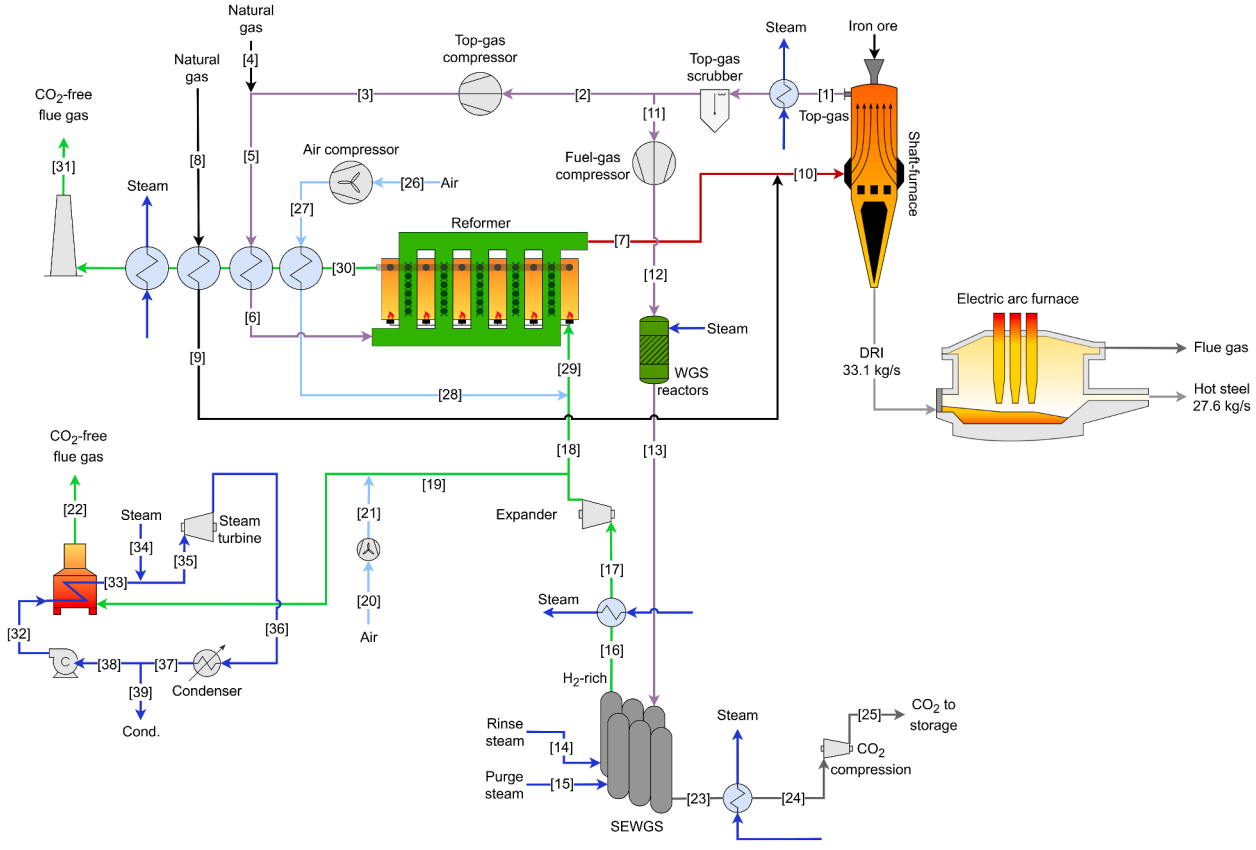

Fig. 4. Midrex plant with pre-combustion carbon capture SEWGS section plus electric arc furnace.

from the top-gas, a H_2-rich stream that can be used as fuel in the reformer. The main differences regard the pressure at which the WGS and the SEWGS reactors are operated but also the lower number of water gas shift reactors needed. Similarly, a split configuration is adopted to reduce the overall consumption of steam in the WGS section (Jansen et al., 2015) (Fig. 7). On the other hand, with respect to DRI-EAF+ MDEA configuration, only two WGS reactors are here considered since the WGS reaction takes place also inside the SEWGS columns. This implies that a lower conversion of CO into CO_2 needs to be reached upstream the carbon capture section. A pre-shift section is in any case necessary to achieve a molar concentration of CO at the inlet of SEWGS between 5% and 10% (Jansen et al., 2015). In the SEWGS the CO_2 is adsorbed on a solid sorbent and removed from the gas phase, shifting the WGS reaction towards the reactants and so enhancing the CO conversion (Jansen et al., 2015). Typically, a potassium promoted hydrotalcite-based material is used (Jansen et al., 2015). The desorption of CO_2 is performed through decreasing of pressure. Some steam needs to be provided to the SEWGS columns in order to reach the desired carbon capture ratio and carbon purity. In addition, the H_2-rich mixture exiting the SEWGS at 18 bar and 400 °C can be expanded in a turbine producing electrical power. Similarly to the other cases the steam necessary for the water gas shift section and the CO_2 capture process is produced exploiting the heat available in the top-gas and in the reformer flue gas. The SEWGS produces a CO_2 stream at 400 °C and at a pressure slightly above atmospheric, giving the possibility to produce some steam by cooling this stream. Furthermore, part of the H_2-rich mixture is used to generate steam and drive a steam turbine. The CO_2-rich stream after being cooled, is compressed up to 78 bar in a multistage compressor, liquefied by cooling to 25 °C and pumped to 110 bar.

An additional top-gas compressor is needed. A three-stage compressor is considered. The intercooling temperature of the first stage is regulated to have a temperature equal to 400 °C at the exit of the second water gas shift. The inlet temperature of the second WGS reactor is set to 340 °C and it is controlled by adding the right amount of steam. This parameter also controls the CO outlet concentration. Similar to the DRI-EAF+ MDEA plant configuration the fuel used in the reformer is very different from the base case, implying a different design of the reformer furnace. On the other hand, the shaft furnace is kept equal to the DRI-EAF case.

3. Methodology

3.1. Thermodynamic assessment

The plants described above have been simulated in Aspen Plus V11, adopting the PENG-ROB method. The ENRTL-RK method has been used only for the carbon capture sections with amines. On the other hand, the electric arc furnace performances were taken from the literature (Demus et al., 2012; Kirschen et al., 2011). The model was calibrated to match the composition and the temperature of the reducing gas at the inlet of the shaft furnace available in literature. In addition, the shaft furnace has been modelled to reproduce the conditions of the top-gas as close as possible to the available plant data. The calibration of the model was carried out setting the following parameters through specific "Design Specs" in Aspen Plus:

- the mass flow rate of the natural gas mixed with the top-gas;
- the mass flow rate of the natural gas directly injected into the shaft furnace;
- the mass flow rate of the natural gas used as fuel in the reformer;
- the heat duty of the reformer;
- the temperature of the top-gas scrubber;
- the top-gas recycling ratio;
- the mass flow rate of the combustion air in order to have a content of oxygen in the flue gas equal to 3%.

The model of the shaft furnace is the same for all the cases as well as the composition, temperature and pressure of the reducing gas. Consequently, composition, temperature and pressure of the top-gas do not vary. The molar composition of natural gas considered in this work is 94.58% CH_4, 1.66% C_2H_6, 0.20% C_3H_8 and 3.56% N_2 with an LHV equal to 47 MJ/kg.

The model of the reformer has been built by adopting a RGibbs reactor, to simulate the steam reforming reaction, and a RStoic reactor to simulate the reformer furnace. The shaft furnace has been simulated mainly with RGibbs and RStoic reactors in order to mimic the reactions occurring in it, while the water gas shift reactors by adopting REquil reactors. The polytropic and the mechanical efficiency of the compressors have been set to 0.8 and 0.95 respectively.

The power consumption of the electric arc furnace and the one of the rolling process considered in this work are taken from literature. The first one is equal to 570 kWh/t_{HRC} (Kirschen et al., 2011) while the latter is equal to 110 kWh/t_{HRC} (Muscolino et al., 2016). The direct emissions of the electric arc furnace are considered equal to 0.1 t_{CO2}/t_{HRC} (Demus et al., 2012) while the ones related to the iron ore production are computed according to the carbon footprint associated with the electricity production and based on values found in (Duarte et al., 2008). The Primary Energy Consumption of the pellets production, used to compute the PEC of the whole DRI-EAF process is equal to 2.58 GJ/t_{HRC} (Sarkar et al., 2018).

3.1.1. Base DRI-EAF plant

In this section the model of the shaft furnace as well as the results of the model calibration are presented and compared to the available data. It is important to underline that the results shown in this section, also hold for the other plant configurations, except for the mass flow rate of the combustion air that slightly varies amongst the cases.

In the shaft furnace the reduction of iron ores takes place. Haematite is reduced by H_2 and CO to metallic iron, forming two intermediate iron oxides: magnetite (Fe_3O_4) and wüstite (FeO) (Hou et al., 2012; Parisi and Laborde, 2004; Vogl et al., 2018; Weiss et al., 2011). The reduction reactions are the following:

$$3Fe_2O_3+H_2 \rightarrow 2Fe_3O_4+H_2O \quad (1)$$

$$3Fe_2O_3+CO \rightarrow 2Fe_3O_4+CO_2 \quad (2)$$

$$Fe_3O_4+H_2 \rightarrow 3FeO+H_2O \quad (3)$$

$$Fe_3O_4 + CO \rightarrow 3FeO + CO_2 \quad (4)$$

$$FeO+H_2 \rightarrow Fe+H_2O \quad (5)$$

$$FeO+CO \rightarrow Fe+CO_2 \quad (6)$$

In addition, also the steam reforming (7), the water gas shift (8), the methane decomposition (9) and the Boudouard (10) reactions take place:

$$CH_4+H_2O \rightleftharpoons CO+3H_2 \quad (7)$$

$$CO+H_2O \rightleftharpoons CO_2+H_2 \quad (8)$$

$$CH_4 \rightleftharpoons C+2H_2 \quad (9)$$

$$2CO \rightleftharpoons C+CO_2 \quad (10)$$

The reactions mentioned above have been included in the model of the shaft furnace. The rest of the plant design parameters have been calibrated to match the composition and the temperature of the reducing gas. The results of this process as well as the comparison between this work and the available data are shown in Table 3 and in Table 4.

The model shows a very good match with the real plant data. Indeed, the relative differences are very small, except for the molar fraction of N_2 and CH_4. On the other hand, these two compounds combined represent less than 5%, reflecting in a negligible error. The obtained results are

also compared to typical values found in literature (Table 5).

3.1.2. DRI-EAF+ MEA plant

When considering the integration of a MEA post-combustion section, the flue gases from the reformer, before being fed to the absorber are first cooled, producing steam. The resulting condensate water is removed. In the absorber the flue gas is in contact with a lean amine stream. The CO_2 is absorbed, and a rich amine stream leaves the bottom of the absorber. This stream is sent to a stripper column to be regenerated. A lean amine stream leaves the reboiler and it is sent back to the absorber while a CO_2-rich streams exits the top of the stripper. The CO_2 stream is compressed in a multi-stage intercooled compressor, cooled to condense water (that is subsequently removed) and finally pumped to the delivery pressure of 110 bar.

The CO_2 capture process has been modelled in Aspen Plus V11 adopting the ENRTL-RK method. The parameters adopted for the system modelling are shown in Table 18, while the main results are listed in Table 6. The electrolyte solution chemistry has been modelled with a "Chemistry" assuming the chemical equilibrium of the following reactions:

Table 2
Data from literature and used for the techno-economic assessment.

Parameter	Unit	Value	Ref
Electric arc furnace power consumption	[kWh/t_{HRC}]	570	(Kirschen et al., 2011)
Rolling process power consumption	[kWh/t_{HRC}]	110	(Muscolino et al., 2016)
Electric arc furnace direct emissions	[t_{CO2}/t_{HRC}]	0.1	(Demus et al., 2012)
Iron ore production emissions (elec. CI = 300 kg/MWh)	[t_{CO2}/t_{HRC}]	0.072	(Duarte et al., 2008)
Iron ore production emissions (elec. CI = 900 kg/MWh)	[t_{CO2}/t_{HRC}]	0.129	(Duarte et al., 2008)
PEC of pellets production	[GJ/t_{HRC}]	2.58	(Sarkar et al., 2018)

Table 3
Reducing gas, top-gas and DRI. Comparison between model results and available data.

Stream	Temperature [°C]	Pressure [bar]	Mole flow rate [kmol/h]	Molar composition [%]					
				H_2	N_2	H_2O	CO	CO_2	CH_4
Reducing gas									
- Literature	957	n.a.	7841	49.66	1.76	4.28	32.71	2.40	9.08
- This work	957	1.8	7846	49.42	1.75	4.31	33.01	2.45	9.06
- Difference [%]	0.0	n.a.	0.1	−0.5	−0.6	0.7	0.9	2.1	−0.2
Top-gas									
- Literature	285	1.42	8611	40.28	1.02	19.03	19.58	17.09	2.95
- This work	295	1.42	8667	40.73	1.58	19.51	18.62	17.07	2.48
- Difference [%]	3.5	0.0	0.7	1.1	55.3	2.5	−4.9	−0.1	−15.8
Stream	Temperature [°C]	Pressure [bar]	Mass flow rate [kg/s]	Mass composition [%]					
				Fe_2O_3	Fe_3O_4	FeO	Fe	C	
DRI									
- Literature	n.a.	n.a.	33.1	0.00	0.00	7.85	90.05	2.10	
- This work	684	1.4	33.1	0.00	0.00	7.68	90.32	2.00	
- Difference [%]	n.a.	n.a.	0.0	0.0	0.0	−2.2	0.3	4.8	

Table 4
Results of the model calibration.

Design variable	Unit	Value
Mass flow rate of the natural gas mixed with the top-gas	[kg/h]	11,801
Mass flow rate of the natural gas directly injected into the shaft furnace	[kg/h]	11,674
Mass flow rate of the natural gas used as fuel for the reformer	[kg/h]	0
Heat duty of the reformer	[MW]	74
Temperature of the top-gas scrubber	[°C]	50
Top-gas recycling ratio	[%]	64
Combustion air mass flow rate	[kg/h]	185,110

Table 5
Comparison between results of this work and values found in literature.

Parameter	Unit	This work	Ref. value	Reference
PEC DRI production	[GJ/t_{DRI}]	9.72	~ 10.5	(Cavaliere, 2019; Remus et al., 2013)
PEC DRI production	[GJ/t_{HRC}]	11.67	11.85	(Sarkar et al., 2018)
PEC whole process	[GJ/t_{HRC}]	18.33	18.54	(Sarkar et al., 2018)
NG consumption	[kmol/t_{DRI}]	11.77	11.15	(Sarkar et al., 2018)
NG consumption	[GJ/t_{DRI}]	9.3	8.9–9.4	(Sarkar et al., 2018)
NG consumption	[Nm^3/t_{DRI}]	264	259–262	(Rechberger et al., 2020)
Electricity consumption	[kWh/t_{DRI}]	78	80–125	(Cavaliere, 2019; Rechberger et al., 2020)

$$MEA^{+}+H_2O \rightleftharpoons MEA+H_3O^{+} \quad (11)$$

$$MEACCO^{-}+H_2O \rightleftharpoons MEA+HCO_3^{-} \quad (12)$$

$$CO_2+2H_2O \rightleftharpoons H_3O^{+}+HCO_3^{-} \quad (13)$$

$$HCO_3^{-}+H_2O \rightleftharpoons H_3O^{+}+CO_3^{2-} \quad (14)$$

$$2H_2O \rightleftharpoons H_3O^{+}+OH^{-} \quad (15)$$

The equilibrium constant of the reactions (11)-(15) is calculated adopting Eq. (16) with the constants listed in Table 17.

$$\ln\left(K_{eq}\right) = A + B/T + C\cdot\ln(T) + D\cdot T + E\cdot\left(\frac{P-P_{ref}}{P_{ref}}\right) \quad (16)$$

Table 6
Main results of the MEA and MDEA carbon capture sections.

Parameter	Unit	MEA	MDEA
Carbon capture ratio	[%]	90	96
CO_2 to storage	[t/h]	47.5	44.6
Amine/H_2O in lean solvent	[%wt]	30/64.5	48.6/50.0
Lean solvent/$CO_{2,in}$	[(kg/h)/(kg/h)]	29.44	16.15
Lean solvent CO_2 loading	[mol_{CO2}/mol_{amine}]	0.255	0.08
Rich solvent CO_2 loading	[mol_{CO2}/mol_{amine}]	0.396	0.325
Reboiler duty	[MW]	50.89	31.42
Energy consumption	[GJ/t_{CO2}]	3.90	2.57
Power consumption (including CO_2 compression)	[MW]	4.36	4.13

Table 7
MDEA and SEWGS cases. Main parameters of the water gas shift section.

	Inlet temperature [°C]	Inlet pressure [bar]	H_2O/CO [-]	CO conversion [%]
MDEA case				
- WGS 1	300	8.00	4.1	85
- WGS 2	320	7.75	3.1	67
- WGS 3	300	7.40	7.3	51
- Overall			2.1	89
SEWGS case				
- WGS 1	300	18.50	4.1	85
- WGS 2	340	18.25	2.2	52
- Overall			1.5	67

3.1.3. DRI-EAF+ MDEA plant

In the case of the adoption of a MDEA pre-combustion carbon capture section, as described in Section 2.3, an upstream water gas shift section is added. A split flow configuration is adopted in order to reduce the overall steam consumption (Jansen et al., 2015). The plant scheme as well as the operating parameters and the performances of the water gas shift section are shown in Table 7 and in Fig. 6.

Regarding the MDEA carbon capture section, the general description presented in the previous section can be extended to this case. Fig. 5 can be taken as reference, with the only difference in the position of the pump, placed, in this case, upstream the cooler and downstream the MDEA/H_2O make-up, as the stripper's working pressure is lower than the absorber's. The main differences are related to the chemical reactions that take place and the performances of the system. The process has been modelled in Aspen Plus V11 adopting the ENRTL-RK method and assuming the chemical equilibrium. A "Chemistry" is adopted and reaction (17) in addition to reactions (13), (14) and (15) is defined. Eq. (16) is adopted to compute the equilibrium constants, along with the values listed in Table 17.

$$MDEA^{+}+H_2O \rightleftharpoons MDEA+H_3O^{+} \quad (17)$$

The assumptions made for the modelling of carbon capture system and the performance obtained are shown in Table 18 and in Table 6 respectively.

3.1.4. Base DRI-EAF+ SEWGS plant

The adoption of the SEWGS as a carbon capture technology, as described in Section 2.4, implies also the integration of a water gas shift section in the plant layout. As can be observed in Fig. 7, the first water gas shift reactor is fed with only 37% of the syngas similarly to the MDEA case. Only two water gas shift reactors are necessary since the CO conversion to CO_2 is completed in the SEWGS columns (Table 7). The SEWGS technology consists of a multi-column system, operated in pressure swing adsorption approach. During the feeding step, the WGS reaction takes place and CO_2 (and H_2S if present) is adsorbed on a potassium promoted hydrotalcite-based material. The sorbent material, in fact, is catalytically active for the WGS reaction and it has adsorption capacity at high temperatures. Once it is near saturation, the adsorbent material is regenerated by reducing the pressure and purging with superheated steam. Rinse steam is used to increase the purity of the CO_2 stream. The operating conditions and performances of the SEWGS technology have been optimised by using a proprietary Matlab model developed by TNO to reach the required carbon capture ratio and the carbon purity minimizing the steam requirements (Boon et al., 2017,

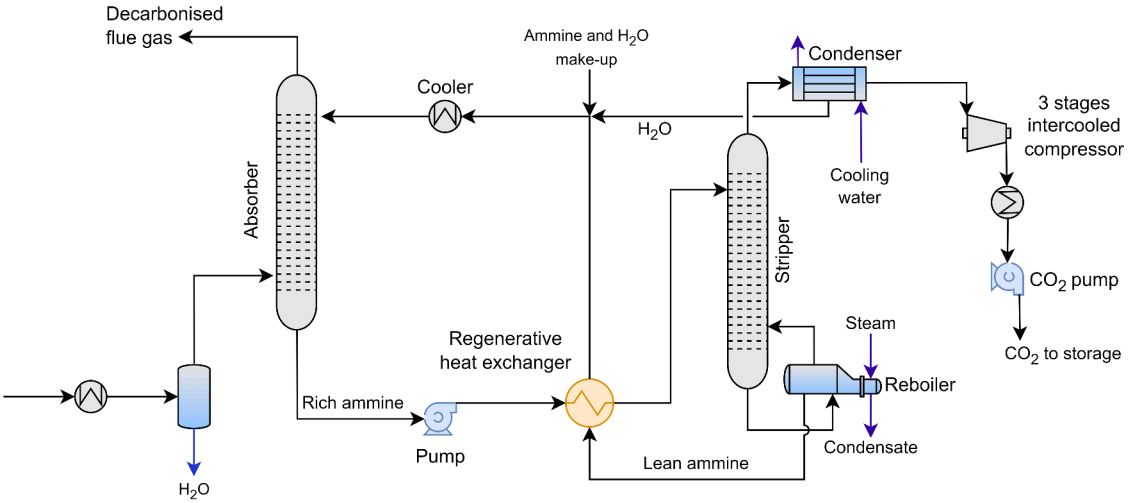

Fig. 5. Layout of the carbon capture section with amine scrubbing and CO_2 compression train.

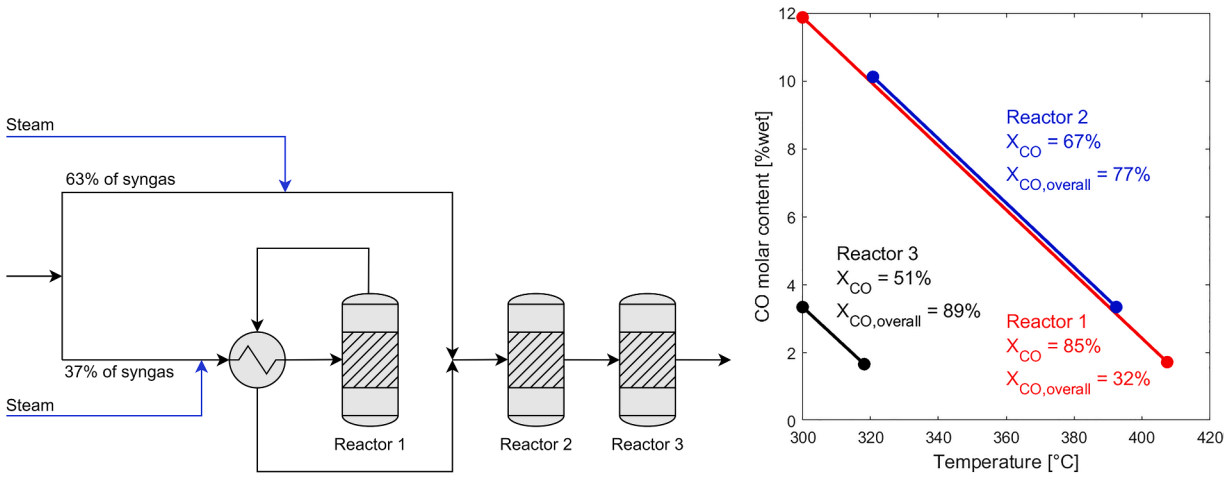

Fig. 6. DRI-EAF + MDEA plant. Schematic of the split configuration adopted in the WGS section (left). Performance in terms of CO conversion of the WGS reactors (right).

2015, 2014). The SEWGS system was modelled in Aspen plus with a specific "Calculator" and using a RStoic reactor (to simulate the WGS reaction) a separator and two heat exchangers. The operating parameters and the performance of the SEWGS are listed in Table 8. The CO_2 stream exiting the SEWGS, as for the other cases, is compressed to 110 bar adopting an intercooled compressor and a pump.

The optimisation of the SEWGS unit focused on optimisation of the cycle design. Various parameters influence the performance: number of columns, size of columns, cycle time, step time, repress composition, and steam amount for rinse and purge. The aim of the optimisation was to identify the cycle design with a reasonable column size and sorbent volume, while keeping the steam amount low. The former influencing CAPEX and OPEX the latter impacting OPEX. In order to increase the productivity of the unit $(mol_{CO_2 captured}/(t_{sorbent}h))$ and thus reduce the sorbent volume, a single train with multiple columns in adsorption was chosen. This design allows to minimise the time between adsorption and desorption while keeping a minimum step length. Furthermore, this design leads to limited gas velocities within the columns, which improve the adsorption kinetics and separation performance. The high hydrogen content within the feed can reduce the net WGS conversion due to thermodynamic constraints compared to other feed gases such as BFG or BOFG, this is counteracted through a feed repress rather than H_2 product repress.

3.2. Economic assessment

The economic assessment was carried out comparing the solutions above described with the reference BF-BOF steel plant (described in the Appendix) and the base DRI-EAF plant. The cost of the raw materials as well as the CAPEX and the fixed OPEX of the DRI-EAF route are taken from (International Energy Agency, 2020) and average values are considered (Table 19). The Total Equipment Cost (TEC) of the additional components (i.e. compressors, reactors, carbon capture sections, etc.) was computed according to the bottom-up methodology described in (Manzolini et al., 2020) using Eq. (18) and the reference costs (C_0), sizes (S_0) and scaling factors (f) reported in Table 20. The Total Plant Cost (TPC) of the additional equipment is then computed taking into account the Total Installation Cost (TIC), the Contingencies (Co) and the Owner's Cost (OC) considering the values indicated in Table 21 (Manzolini et al., 2020). Furthermore, for the MDEA and the SEWGS cases, in order to take

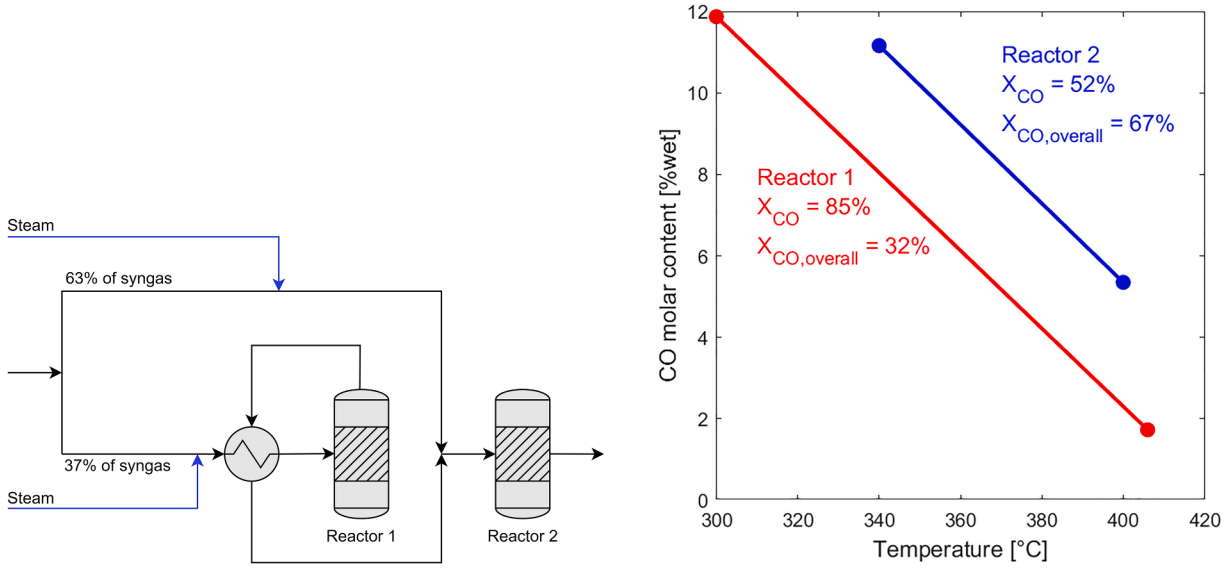

Fig. 7. DRI-EAF + SEWGS plant. Schematic of the split configuration adopted in the WGS section (left). Performance in terms of CO conversion of the WGS reactors (right).

Table 8
SEWGS operating parameters and performances.

Parameter	Unit	Value
Number of trains	[-]	1
Number of columns per train	[-]	20
Column diameter	[m]	2.31
Column height	[m]	7.44
Sorbent lifetime	[years]	5
Feed stream pressure	[bar]	18
Feed stream temperature	[°C]	400
Feed stream CO molar fraction	[-]	5.3
Feed stream CO+CO_2 content	[kmol/h]	1106
Rinse steam pressure	[bar]	18
Rinse steam temperature	[°C]	400
Rinse steam consumption	[$kmol_{H2O}$/$kmol_{CO+CO2}$]	0.29
Purge steam pressure	[bar]	2
Purge steam temperature	[°C]	400
Purge steam consumption	[$kmol_{H2O}$/$kmol_{CO+CO2}$]	0.80
CO_2 purity	[%]	98.85
CO_2 capture ratio	[%]	92.1
Power consumption (including CO_2 compression)	[MW]	4.79

into account the different layout of the reformer furnace (as described in Section 2.3 and 2.4) an additional cost equal to 5% of the CAPEX of the base DRI-EAF plant has been considered. Additional assumptions made to carry out the economic assessment are shown in Table 19.

$$C_{e,i} = n \cdot C_{0,i} \left(\frac{S_{e,i}}{n \cdot S_{0,i}} \right)^{f} \tag{18}$$

In the case of the reference BF-BOF steel plant, the economic assessment is carried out adapting the costs of a 4 Mt_{HRC}/y plant, found in (Manzolini et al., 2020), to the current case. The steel mill plant cost without the power plant and the "total other costs" have been scaled on the basis of the plants' sizes through Eq. (18) with a scaling factor equal to 0.67. The "total fixed O&M", and the "total miscellaneous" have been computed as a percentage of the steel mill plant cost. The same percentages used in (Manzolini et al., 2020) have been considered. The "total variable O&M" have been scaled linearly keeping the plants' size as scaling parameter. The results are shown in Table 9.

The cost of the combined cycle integrated in the steel plant is computed through Eq. (18) following the methodology described above and using the values reported in Table 20 (considering two gas turbines and two fuel compressors). Once the TEC of the combined cycle is computed, the total plant cost of the power block can be estimated with the values listed in Table 21 and added to the costs described in the previous paragraph to compute the TPC of the integrated steel mill.

3.3. Key performance indicators

The comparison between all the different cases investigated is made through economic and environmental Key Performance Indicators (KPIs) typical of this analysis and available in (Gentile et al., 2022; Khallaghi et al., 2022; Manzolini et al., 2020). Being the KPIs computed per ton of HRC, the comparison amongst plants with different sizes (3.16 Mt_{HRC}/y for BF-BOF route and 0.814 Mt_{HRC}/y for the DRI-EAF plants) can be carried out. The environmental indexes considered in this study are: the Primary Energy Consumption (PEC), the specific CO_2 emissions (e_{CO2}), the CO_2 Capture Ratio (CCR), the Specific Primary Energy Consumption for CO_2 Avoided (SPECCA) and the CO_2 Avoidance (CA). The SPECCA indicator is defined as the additional primary energy required (in GJ) to avoid the emission of 1 ton of CO_2 producing the same amount of product.

Table 9
Main economic results of the BF-BOF plant without power generation block.

Item	Unit	Value
Steel size	[Mt_{HRC}/y]	3.16
TPC w/o power generation block	[M€]	3548.8
Total fixed O&M	[M€/y]	317.2
Total variable O&M	[M€/y]	742.5
Total miscellaneous	[M€]	44.0
Total other costs	[M€]	8.4

$$PEC\left[\frac{GJ}{t_{HRC}}\right] = \frac{\dot{m}_{fuel} LHV_{fuel} + \dot{W}_{el}\left(\dot{W}_{fuel}/\dot{W}_{el}\right) + \dot{Q}_{req}/\eta_{th}}{\dot{m}_{HRC}} \tag{19}$$

$$e_{CO_2}\left[\frac{t_{CO_2}}{t_{HRC}}\right] = \frac{\dot{m}_{CO_2}}{\dot{m}_{HRC}} \tag{20}$$

$$CCR[\%] = \left(1 - \dot{m}_{CO_2,out}/\dot{m}_{CO_2,in}\right) \cdot 100 \tag{21}$$

$$SPECCA\left[\frac{GJ}{t_{CO_2}}\right] = \frac{PEC_{capture} - PEC_{no\ capture}}{e_{CO_2,no\ capture} - e_{CO_2,capture}} \tag{22}$$

$$CA[\%] = \left(\frac{e_{CO_2,no\ capture} - e_{CO_2,capture}}{e_{CO_2,no\ capture}}\right) \cdot 100 \tag{23}$$

In this study, the PEC associated to the electricity generation has been computed in relation to its carbon footprint, taking the values shown in Table 10 as reference, and linearly interpolating them for intermediate cases. When the carbon intensity of the electricity imported from the grid is equal to 0 kg_{CO2}/MWh_e, so in the renewable energy scenario, no fossil fuels are consumed, and the PEC associated to electricity generation is considered to be equal to 0 MWh_{LHV}/MWh_e. When the electricity carbon intensity is equal to 350 kg_{CO2}/MWh_e it is supposed that the electricity is produced in a NGCC with an efficiency (η_e) of 60%. Last considered case is the coal ultra-supercritical cycle, having an efficiency (η_e) equal to 42% and a carbon footprint of 850 kg_{CO2}/MWh_e. The PEC associated to the electricity generation in the two previously mentioned power plants is then computed as $1/\eta_e$.

The economic performance is assessed in terms of Levelised Cost of Hot Rolled Coil (LCOHRC) and Cost of CO_2 avoided (CCA). The Total Annualized Cost (TAC) is computed considering the Total Plant Cost (TPC), annualised through the Fixed Charge Rate (FCR), the variable (C_v) and the fixed (C_f) costs.

$$LCOHRC\left[\frac{€}{t_{HRC}}\right] = \frac{TAC}{\dot{m}_{HRC} \cdot 8760 \cdot \tau} \cdot 10^6 \tag{24}$$

$$TAC\left[\frac{M€}{y}\right] = TPC \cdot FCR + C_v + C_f \tag{25}$$

$$FCR = \frac{r(1+r)^T}{(1+r)^T - 1} \tag{26}$$

$$CCA\left[\frac{€}{t_{CO_2}}\right] = \frac{TAC_{capture} - TAC_{no\ capture}}{e_{CO_2,no\ capture} - e_{CO_2,capture}} \tag{27}$$

Where (τ) is the plants' availability, (r) the interest rate and (T) the plants' lifetime.

4. Results

The main results of the energy, environmental, and economic

Table 10
PEC of electricity generation.

Parameter	Unit	RES	NGCC	Coal USC
Electricity C.I.	[kg_{CO2}/MWh_e]	0	350	850
Cycle efficiency	[MW_e/MW_{LHV}]	–	60	42
PEC electricity generation	[MWh_{LHV}/MWh_e]	0	1.67	2.38

assessment are presented in this section. A sensitivity analysis on natural gas price and electricity price is also performed.

4.1. Environmental results

In Sections 4.1.1 and 4.1.2 the environmental results considering an electricity carbon footprint of 350 kg_{CO2}/MWh are shown. Since this parameter affect both the CO_2 emissions and the PEC, a sensitivity analysis is performed and it is described in Section 4.1.3.

4.1.1. Reference BF-BOF plant

The BF-BOF steel mill consumes 6240 t/d of coal while the plant electricity requirement is entirely fulfilled by the integrated combined cycle. The CO_2 direct emissions amount to 1.972 t_{CO2}/t_{HRC} to which indirect emissions related to iron ore production must be added. These upstream emissions vary with the electricity carbon footprint. The total CO_2 emissions thus are equal to 2.049 t_{CO2}/t_{HRC}. The resulting PEC is equal to 21.93 GJ/t_{HRC}, related to coal consumption and it is independent of the carbon footprint of electricity production since all the electricity necessary to run the integrated steel mill is internally produced.

4.1.2. DRI-EAF plants

The electric power consumption of the base DRI-EAF plant, as a result of the Aspen simulation, is 9.23 MW_e, corresponding to 78 kWh/t_{DRI}. It is estimated that the top-gas compressor consumes 4.35 MW_e while the air blower 4.89 MW_e. The whole natural gas input amounts to 23.5 t/h (9.26 GJ/t_{DRI}).

In the case of the plants with the integration of a carbon capture technology, additional natural gas and electricity are consumed with respect to the base DRI-EAF plant. Additional natural gas may be needed to generate the steam necessary to regenerate the solvents if the waste heat is not sufficient. Similarly, an increase of electricity demand is due to the compression of the captured CO_2 as well as to run additional equipment. The electricity requirements, the PEC associated to the processes and the CO_2 emissions are reported in Table 11. The MDEA case is the one with the highest power consumption. In fact, an additional compressor is installed upstream the WGS section, increasing the power requirement of the plant. Differently from the SEWGS case, it is not possible to install an expander downstream the carbon capture section to produce power since the treated gas leaves the absorber at low temperature. On the other hand, in the SEWGS case, the H_2-rich stream leaves the carbon capture section at 400 °C and 18 bar making possible to exploit it to generate electricity. In the case of the MEA plant, additional natural gas, corresponding to 0.51 GJ/t_{DRI} must be imported. Regarding the MDEA plant this value drops to 0.24 GJ/t_{DRI} while for the SEWGS plant, the waste heat available is sufficient to provide steam for the WGS reactors and the SEWGS itself. This leads to almost same value of PEC for the MEA and MDEA cases and a lower PEC for the SEWGS case. Regarding the emissions of the whole process the SEWGS plant has the best performance. The results are summarised in Table 11. The primary energy consumption of the DRI-EAF plants is represented in Fig. 8 and it is compared to the BF-BOF case (black line). The "CO_2 capture" (Fig. 8, right) includes the "CO_2 compression" work, the "additional electricity" and the "additional natural gas".

4.1.3. Sensitivity analysis on carbon footprint of imported electricity

The so far presented results have been computed considering the carbon footprint of the electricity being 350 kg_{CO2}/MWh. A sensitivity analysis on this parameter is presented in this section since it directly affects all the environmental KPIs as explained in paragraph 3.3. Indeed, the primary energy consumption associated to electricity generation is considered equal to zero for a renewable energy scenario (i.e. electricity carbon footprint equal to 0 kg_{CO2}/MWh) since no fossil fuels are consumed but it increases with the electricity carbon footprint. Consequently, the higher the electricity carbon footprint, the higher the PEC and the CO_2 emissions of the DRI-EAF plants. The BF-BOF route is

Table 11
DRI-EAF plants energy balance.

Plant balance	Unit	DRI-EAF	MEA	MDEA	SEWGS
Electricity balance:					
- Top-gas compressor	[kW]	4347	4818	4817	4818
- Main Air blower	[kW]	4887	4887	4887	4692
- CO_2 compression train	[kW]	–	4364	4127	4719
- Fuel gas compressor	[kW]	–	–	5972	9211
- Combustion air blower	[kW]	–	138	64	–
- H_2 expander	[kW]	–	–	–	−4381
- Steam turbine	[kW]	–	–	–	−3217
- EAF	[kW]	67,879	67,879	67,879	67,879
- Rolling	[kW]	13,100	13,100	13,100	13,100
- Overall electricity balance	[kW]	90,213	95,186	100,847	96,820
NG consumption	[kg/s]	6.52	6.88	6.69	6.52
NG consumption	[MW]	306	323	314	306
DRI produced	[kg/h]	33.08	33.08	33.08	33.08
Electricity consumption:					
- DRI production	[kWh/t_{DRI}]	77.5	81.5	81.5	79.9
- CO_2 compression	[kWh/t_{DRI}]	0.0	36.6	34.7	39.6
- Additional equipment	[kWh/t_{DRI}]	0.0	1.2	50.7	13.5
- Overall electricity consumption	[kWh/t_{DRI}]	77.5	119.3	166.8	133.0
Primary energy consumption:					
- Pellets production	[GJ/t_{HRC}]	2.58	2.58	2.58	2.58
- Natural gas (DRI production)	[GJ/t_{HRC}]	11.11	11.11	11.11	11.11
- Electricity (DRI production)	[GJ/t_{HRC}]	0.56	0.59	0.59	0.57
- Electric arc furnace	[GJ/t_{HRC}]	3.42	3.42	3.42	3.42
- Rolling	[GJ/t_{HRC}]	0.66	0.66	0.66	0.66
- CO_2 capture	[GJ/t_{HRC}]	0.00	0.88	0.90	0.38
- Overall PEC	[GJ/t_{HRC}]	18.33	19.23	19.26	18.73
CO_2 emissions:					
- Pellets production	[t_{CO2}/t_{HRC}]	0.077	0.077	0.077	0.077
- DRI production	[t_{CO2}/t_{HRC}]	0.557	0.137	0.168	0.131
- Electric arc furnace	[t_{CO2}/t_{HRC}]	0.300	0.300	0.300	0.300
- Rolling	[t_{CO2}/t_{HRC}]	0.039	0.039	0.039	0.039
- Overall CO_2 emissions	[t_{CO2}/t_{HRC}]	0.972	0.551	0.583	0.546

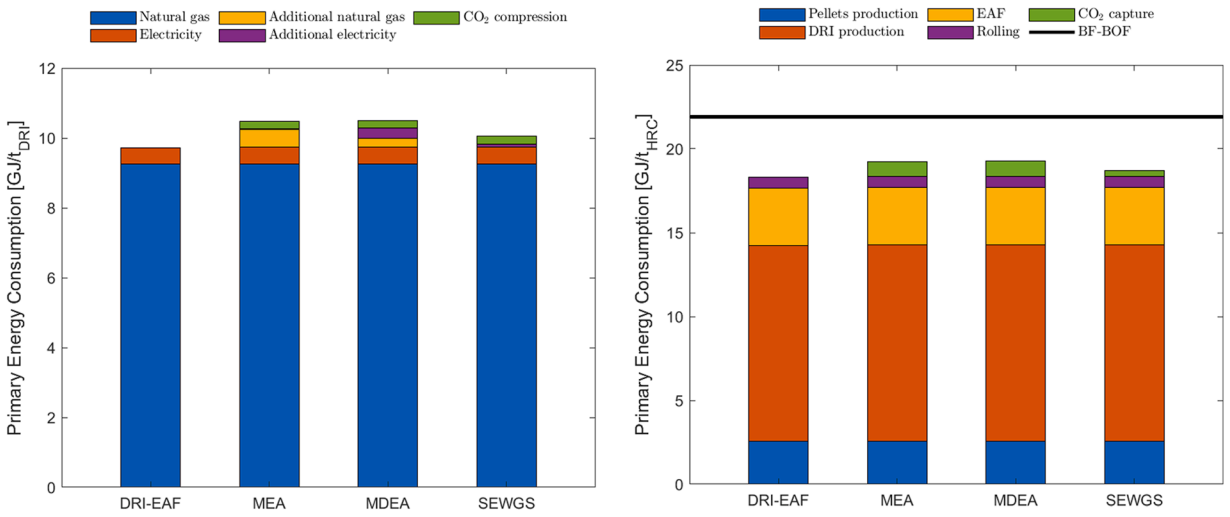

Fig. 8. Primary energy consumption of the DRI-EAF plants computed per ton of DRI (left) and per ton of HRC (right).

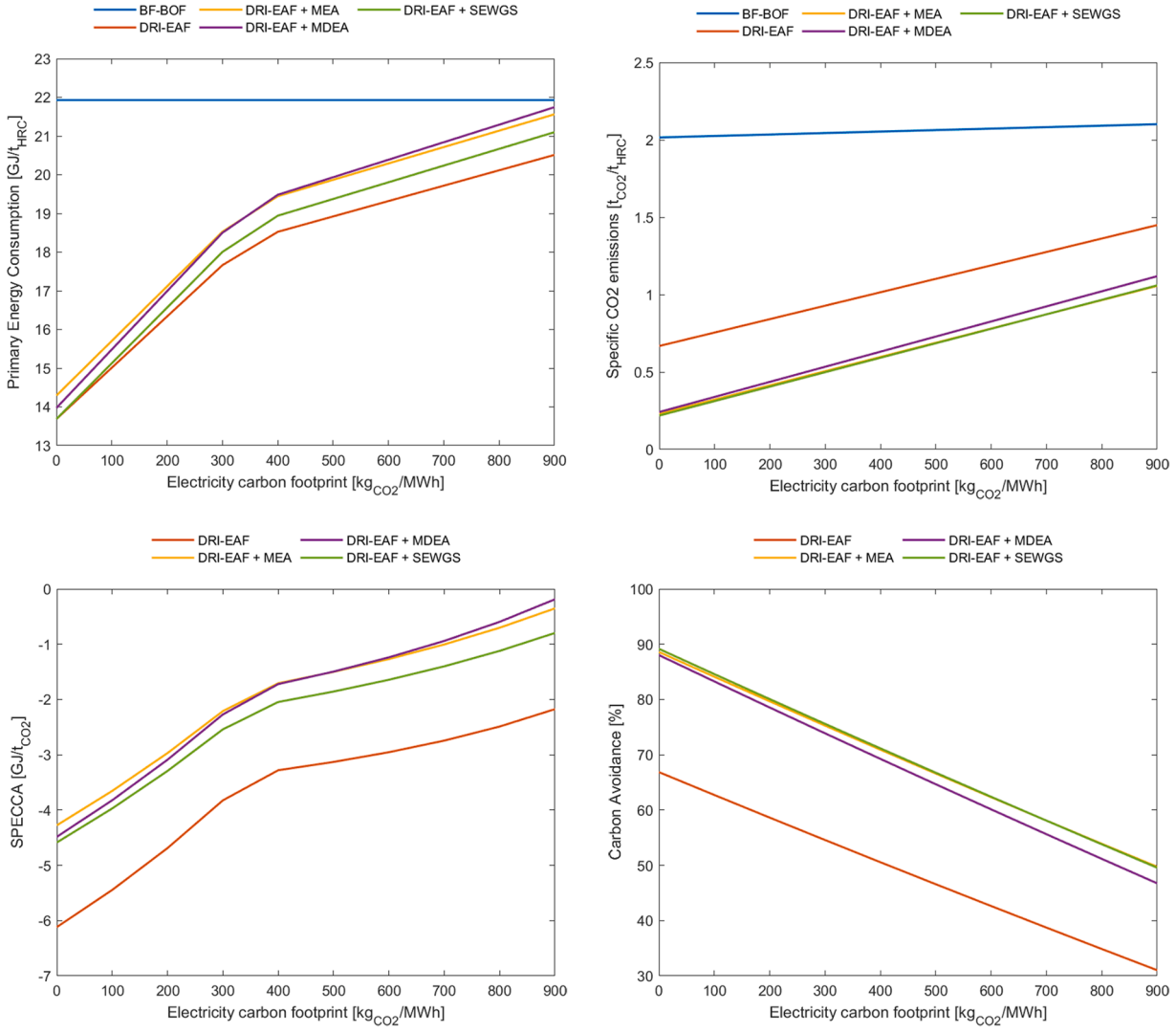

Fig. 9. PEC, specific CO_2 emissions, SPECCA and CA for the analysed plants.

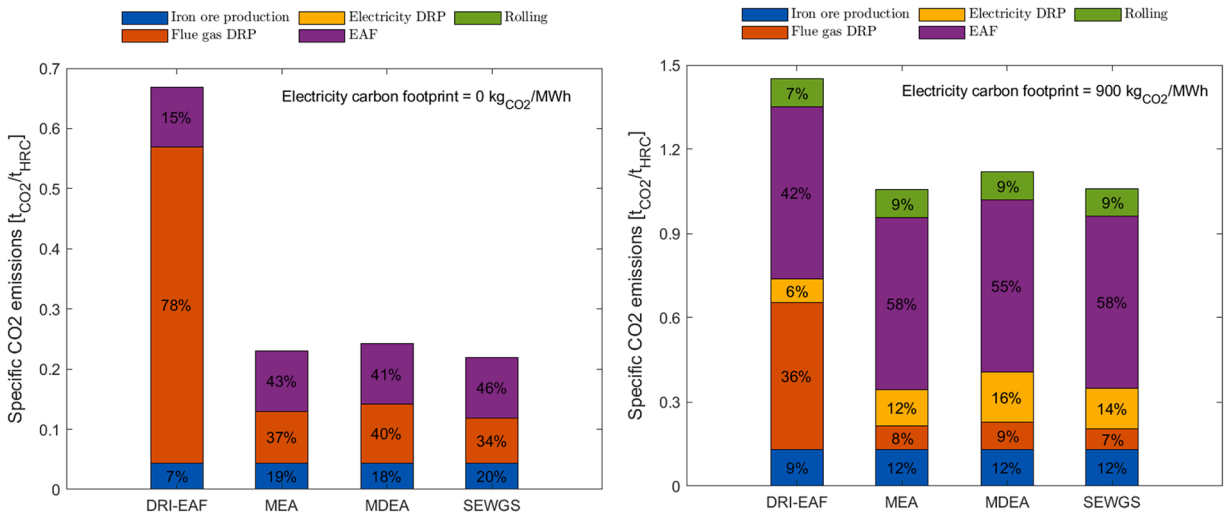

Fig. 10. CO_2 emissions breakdown of the DRI-EAF plants for a carbon footprint of electricity equal to 0 kg_{CO2}/MWh (left) and 900 kg/MWh (right).

Table 12
Breakdown of LCOHRC for the DRI-EAF plants.

Parameter	Unit	DRI-EAF	MEA	MDEA	SEWGS
LCOHRC	[€/t_{HRC}]	616.81	656.80	671.33	656.70
- Annualised Capex	[€/t_{HRC}]	86.94	94.53	104.84	101.50
- Fixed Cost	[€/t_{HRC}]	79.58	82.78	85.29	83.88
- Iron ore	[€/t_{HRC}]	112.18	112.18	112.18	112.18
- Electricity	[€/t_{HRC}]	115.96	123.47	132.03	125.94
- Natural gas	[€/t_{HRC}]	222.15	234.29	227.89	222.15
- Other variable costs	[€/t_{HRC}]	0.00	9.54	9.10	11.04
CCA	[€/t_{CO2}]	122.41	114.73	127.09	114.23

slightly affected by this parameter, since it has an impact only on the emissions related to the iron ore production, giving that no electricity is imported to run the steel mill.

The DRI-EAF+ SEWGS plant imports the same quantity of natural gas but a higher quantity of electricity with respect to the DRI-EAF base plant. For this reason, when renewable energy is considered, the PEC of the two plants is equal (Fig. 9). In all the scenarios the PEC of DRI-EAF plants is lower than the one of the BF-BOF route, reflected in a negative SPECCA, meaning that less primary energy is consumed to produce the same amount of steel while reducing the CO_2 emissions. The MEA, MDEA and SEWGS cases show very similar values of carbon avoidance, with the SEWGS plant performing slightly better and reaching almost 90% with respect to the BF-BOF route when the renewable energy scenario is considered. Generally, the DRI-EAF+ SEWGS shows the best KPIs. The advantage of the SEWGS plant with respect to the other two DRI-EAF plants equipped with a carbon capture technology is given by the lower consumption of natural gas.

The breakdown of the CO_2 emissions of the DRI-EAF plants with the relative weight, expressed in percentages, of the different contributions to the whole emissions is shown in Fig. 10. The two extreme cases are shown, the renewable one (left side) and the case in which the carbon footprint of electricity is equal to 900 kg_{CO2}/MWh (right side).

4.2. Economic results

The economic assessment shows that the BF-BOF plant has the lowest LCOHRC being equal to 485 €/t_{HRC}. In the case of the DRI-EAF plants, the breakdown of the LCOHRC is shown in Table 12. "Other variable costs" include the CO_2 transport and storage, the amine/water make-up for MEA and MDEA cases and the sorbent cost for the SEWGS case. As can be observed (Table 12 and Fig. 11) the higher CAPEX of the SEWGS case is compensated by the lower import of natural gas leading to LCOHRC slightly lower than the MEA case, while the MDEA plant shows

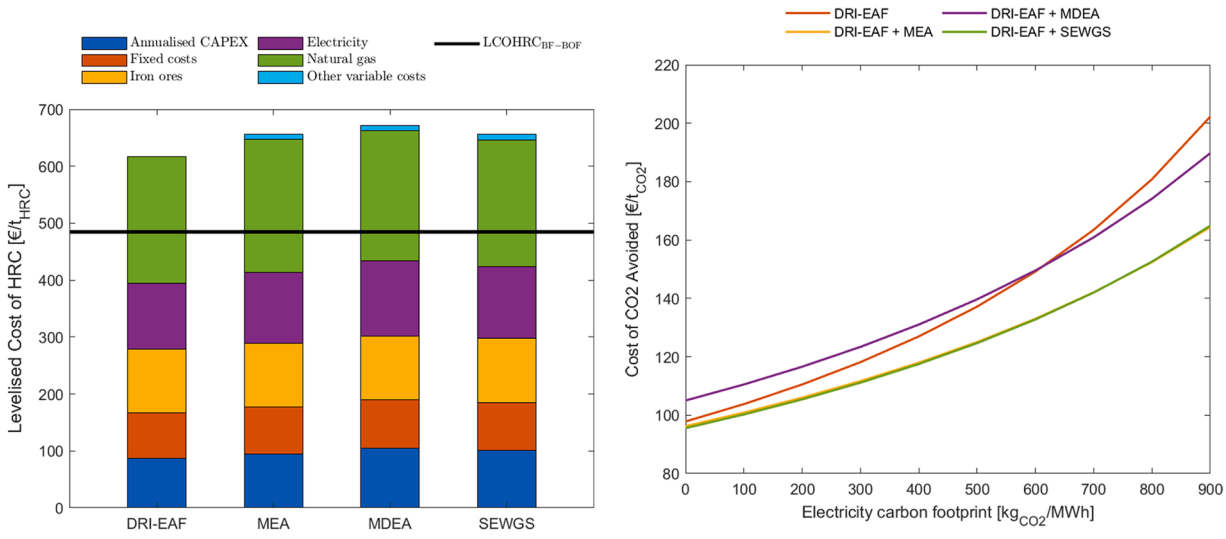

Fig. 11. LCOHRC of the DRI-EAF plants (left) and CCA (right).

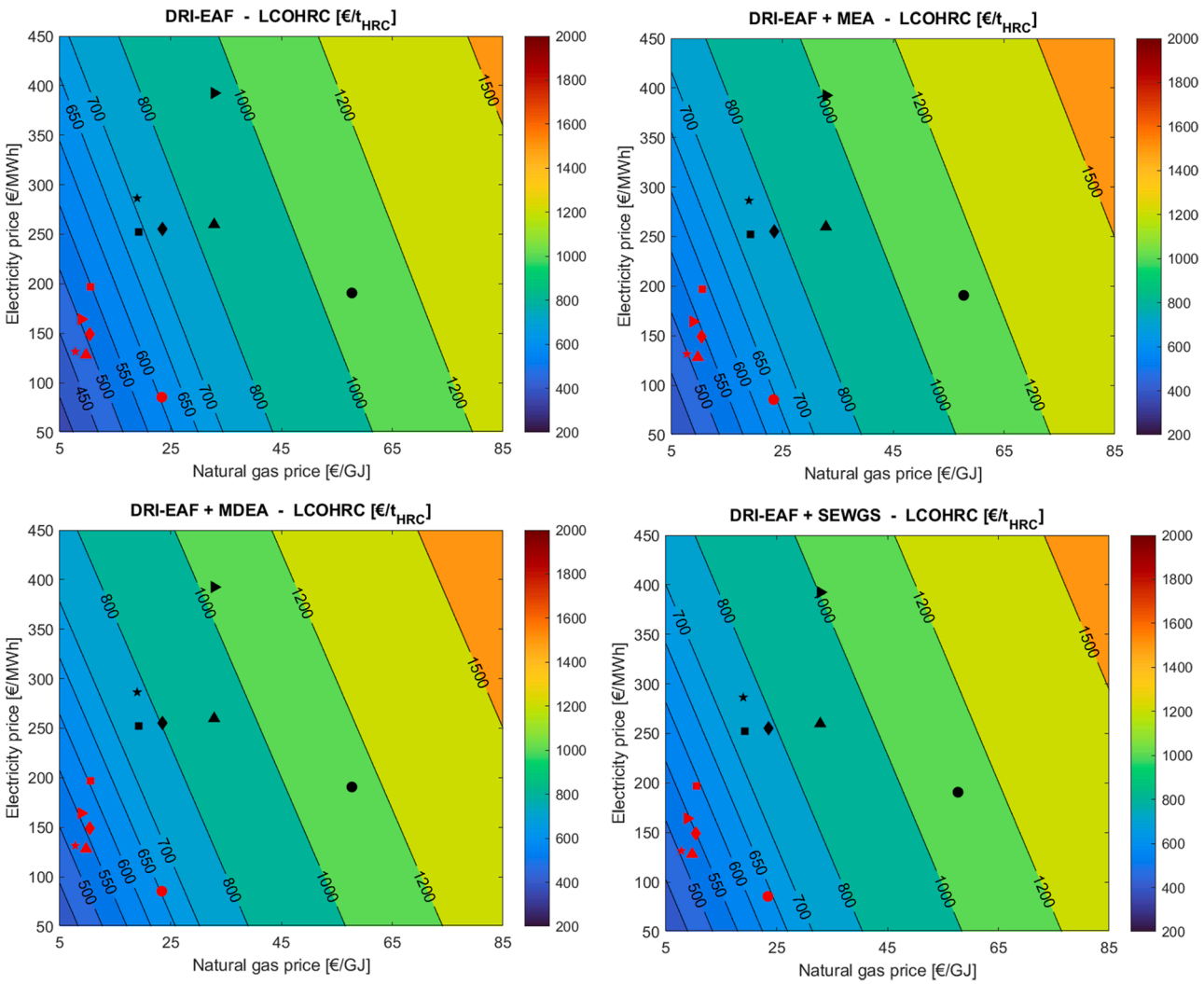

Fig. 12. LCOHRC for the DRI-EAF plants computed varying the natural gas and the electricity prices.

the highest LCOHRC. The costs associated to natural gas and to electricity purchase represent a large fraction of the LCOHRC. The cost of CO_2 avoided of the SEWGS and MEA plants is very similar, and it is even lower than the one of the DRI-EAF base case. This KPI is represented in Fig. 11 against the carbon footprint of the electricity imported.

4.2.1. Sensitivity analysis on natural gas and electricity price

As observed in the previous section the electricity price and especially the natural gas price strongly impact on the LCOHRC. For this reason, a sensitivity analysis on these parameters was carried out by varying the natural gas price between 5 and 85 €/GJ and the electricity price between 50 and 450 €/MWh. In addition, the curve cost for the DRI-EAF plants was obtained:

$$LCOHRC_{DRI-EAF} = 278.70 + 0.773 \cdot c_{el} + 11.11 \cdot c_{NG} \quad (28)$$

$$LCOHRC_{MEA} = 299.03 + 0.823 \cdot c_{el} + 11.71 \cdot c_{NG} \quad (29)$$

$$LCOHRC_{MDEA} = 311.41 + 0.880 \cdot c_{el} + 11.39 \cdot c_{NG} \quad (30)$$

$$LCOHRC_{SEWGS} = 308.61 + 0.840 \cdot c_{el} + 11.11 \cdot c_{NG} \quad (31)$$

with the electricity price (c_{el}) and the natural gas price (c_{NG}) expressed in €/MWh and €/GJ respectively.

The LCOHRC have been computed for five different European countries (Sweden, Italy, Germany, Spain and Belgium) and for a case representing the average of the Eurozone, using the natural gas and the electricity prices in 2018 and in 2022 (https://ec.europa.eu/eurostat).

The results of the sensitivity analysis are shown in Fig. 12, where a colour map of the LCOHRC for each DRI-EAF plant is represented. The colour nuances vary from blue (lowest values of LCOHRC) to red (highest values of LCOHRC). The DRI-EAF+ SEWGS plant presents the best results amongst the plants with the integration of a carbon capture technology. In some limited regions, the LCOHRC of the DRI-EAF plants is lower than the LCOHRC of the BF-BOF plant.

Similarly, varying the natural gas and the electricity prices, the cost of CO_2 avoided has been computed (Fig. 13). A carbon footprint of electricity equal to 350 kg_{CO2}/MWh has been considered. This parameter affects the DRI-EAF plants carbon avoidance with respect to the BF-BOF steel mill and thus the CCA. The region with the darkest nuance of blue is the one with a negative CCA. This figure also gives an idea of the CO_2 tax that would need to be implemented such that the LCOHRC of the DRI-EAF plants would be the same of the BF-BOF plant. In addition, the CCA was computed for the same countries and years mentioned above. The results are shown in Fig. 13.

5. Conclusion

The iron and steel industry is amongst the most carbon intensive and energy intensive sectors. This work discusses the techno-economic assessment of the integration of the SEWGS technology in a Midrex-

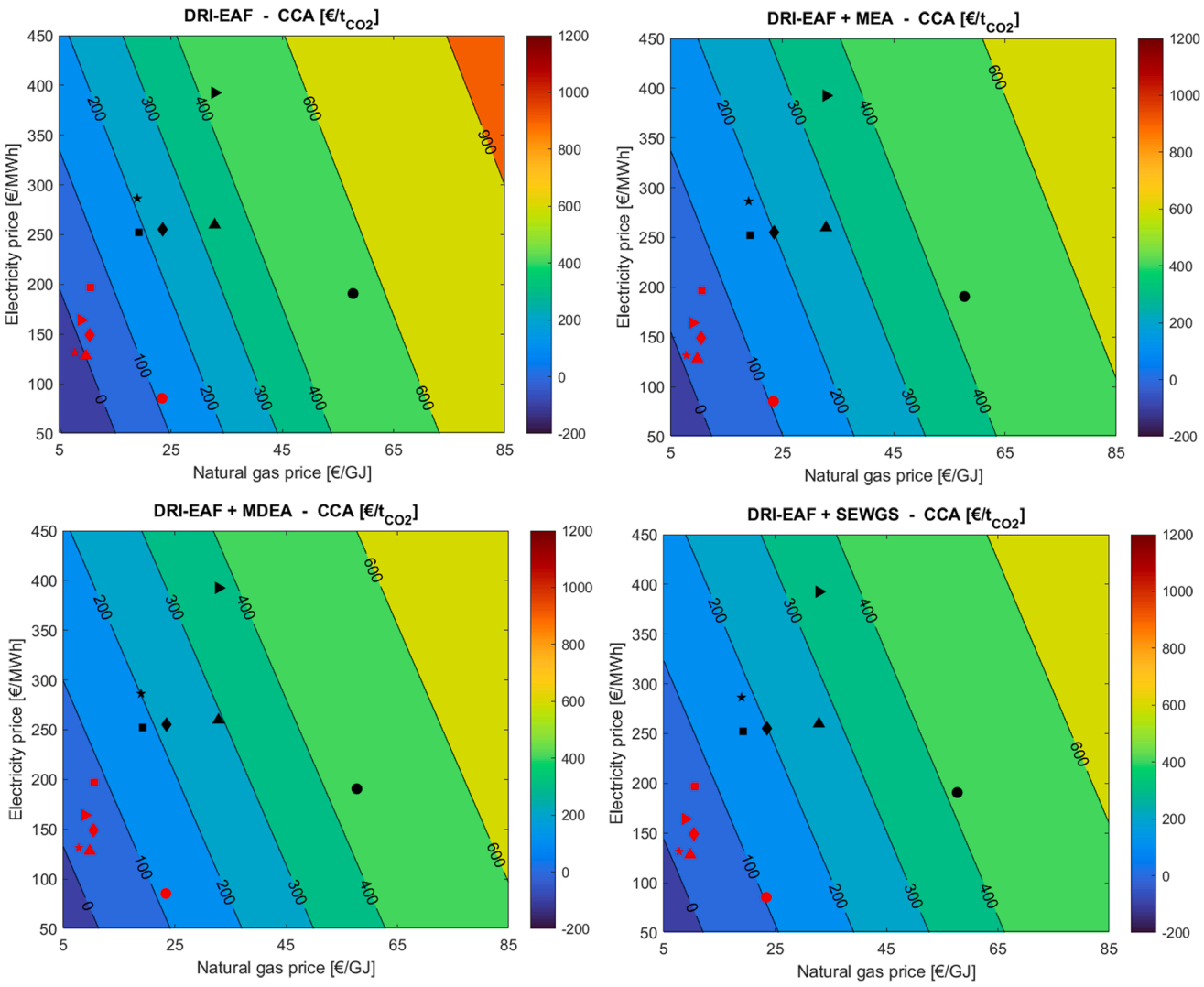

Fig. 13. CCA for the DRI-EAF plants computed varying the natural gas and the electricity prices.

EAF plant for GHG mitigation of the steelmaking sector. The analysis is carried out by comparing different plants through economic and environmental KPIs with respect to the BF-BOF route. Real plant data, available in literature, have been used to model a Midrex-EAF plant. The same data have been used to investigate the possibility of reducing the carbon footprint of the DRI-EAF route by adopting 3 different technologies: (i) MEA post-combustion, (ii) MDEA pre-combustion and (iii) the SEWGS pre-combustion technology. The reduction of CO_2 emissions was focused on the DR process while keeping the EAF and the other steps as is. The introduction of carbon capture technologies increases the PEC but considerably reduces the carbon footprint of the process. In general, the DRI-EAF route presents a primary energy consumption and CO_2 emissions lower than the reference BF-BOF plant. The MEA and SEWGS cases show similar KPIs, with the SEWGS having lower PEC and SPECCA due to the lower import of natural gas. The lower import of natural gas represents an advantage towards the SEWGS solution. Quantification of the KPIs indicates that the MDEA case underperforms with respect to the other CCS cases. In the renewable energy scenario, the MEA and SEWGS cases reach a carbon avoidance close to 90% with respect to the BF-BOF route.

By an economic point of view, the LCOHRC of the DRI-EAF plant (616.81 €/t_{HRC}) is 27% higher than the BF-BOF case (485.00 €/t_{HRC}). The adoption of carbon capture technologies increases the LCOHRC of the DRI-EAF route, by 6.5%, 6.5% and 8.8% in the case of SEWGS (656.70 €/t_{HRC}), MEA (656.80 €/t_{HRC}) and MDEA (671.33 €/t_{HRC}) respectively. On the other hand, it has to be underlined that the natural gas and the electricity prices have a strong impact on the LCOHRC of the DRI-EAF route. For this reason, a sensitivity analysis on these two parameters was carried out, showing that in some regions of the price maps the LCOHRC of the DRI-EAF route is even lower than the LCOHRC of the BF-BOF case. Similarly, also the CCA has been calculated, showing negative values in the above-mentioned regions.

The carbon footprint associated to the electricity generation directly affects the emissions of the plants and therefore the CCA. Assuming a natural gas price of 20 €/GJ and an electricity price of 150 €/MWh, the CCA varies between 95 €/t_{CO2} (electricity carbon intensity: 0 kg_{CO2}/MWh) and 164 €/t_{CO2} (electricity carbon intensity: 900 kg_{CO2}/MWh) for the MEA and the SEWGS cases.

Furthermore, in the proposed low-carbon configurations, only little modifications have to be introduced with respect to the base DRI-EAF plant. In fact, in all the cases, a conventional shaft-furnace can be adopted being always fed with the same reducing gases. The only equipment that has to be differently designed is the furnace of the reformer for the MDEA and SEWGS cases where a H_2-rich fuel is used.

Finally, considering that the DRI-EAF route is already globally adopted on industrial scale, the commercial integration of low carbon configurations could be probably viable in the next future, contributing to the decarbonisation of the steel sector.

CRediT authorship contribution statement

Nicola Zecca: Conceptualization, Methodology, Software, Validation, Formal analysis, Investigation, Data curation, Writing – original draft. **Paul D. Cobden:** Conceptualization, Writing – review & editing, Supervision. **Leonie Lücking:** Software, Writing – review & editing. **Giampaolo Manzolini:** Conceptualization, Methodology, Writing – review & editing, Supervision, Funding acquisition.

Declaration of Competing Interest

The authors declare that they have no known competing financial interests or personal relationships that could have appeared to influence the work reported in this paper.

Data availability

Data will be made available on request.

Acknowledgments

This paper is part of the INITIATE project that has received funding from the European Union's Horizon 2020 research and innovation programme under grant agreement N 958318.

Appendix

Streams specifications of the DRI-EAF plants

The mass balance and the thermodynamic properties of the streams in the DRI-EAF plants are shown in Table 13 (base DRI-EAF), Table 14 (DRI-EAF + MEA), Table 15 (DRI-EAF + MDEA) and Table 16 (DRI-EAF + SEWGS).

Table 13
Main streams specifications of the base DRI-EAF plant.

Stream	Temperature [°C]	Pressure [bar]	Mass flow rate [kg/s]	Molar composition [%]									
				H_2O	H_2	CO	CO_2	N_2	CH_4	C_2H_6	C_3H_8	O_2	Ar
1	298	1.42	43.1	19.51	40.73	18.62	17.07	1.58	2.48	–	–	–	-
2	50	1.42	24.1	7.70	46.71	21.36	19.58	1.82	2.85	–	–	–	-
3	146	3.00	24.1	7.70	46.71	21.36	19.58	1.82	2.85	–	–	–	-
4	45	2.50	3.3	–	–	–	-	3.56	94.58	1.66	0.20	–	-
5	131	2.50	27.4	6.72	40.79	18.65	17.10	2.04	14.47	0.21	0.03	–	–
6	610	2.00	27.4	6.72	40.79	18.65	17.10	2.04	14.47	0.21	0.03	–	-
7	1055	1.80	27.4	4.73	54.24	36.23	2.69	1.58	0.53	–	–	–	-
8	45	2.50	3.2	–	–	–	-	3.56	94.58	1.66	0.20	–	-
9	480	2.00	3.2	–	–	–	-	3.56	94.58	1.66	0.20	–	-
10	957	1.80	30.7	4.31	49.42	33.01	2.45	1.75	8.90	0.15	0.02	–	–
11	50	1.42	13.4	7.70	46.71	21.36	19.58	1.82	2.85	–	–	–	-
12	15	1.01	51.4	–	–	–	0.03	78.03	–	–	–	20.99	0.95
13	100	2.00	51.4	–	–	–	0.03	78.03	–	–	–	20.99	0.95
14	610	1.50	51.4	–	–	–	0.03	78.03	–	–	–	20.99	0.95
15	438	1.42	64.8	2.29	13.88	6.35	5.84	55.38	0.85	–	–	14.75	0.67
16	1132	1.42	64.8	19.87	–	–	14.50	61.61	–	–	–	3.28	0.74
17	440	1.12	64.8	19.87	-	-	14.50	61.61	-	-	-	3.28	0.74

Table 14
Main streams specifications of the DRI-EAF+ MEA plant.

Stream	Temperature [°C]	Pressure [bar]	Mass flow rate [kg/s]	Molar composition [%]									
				H_2O	H_2	CO	CO_2	N_2	CH_4	C_2H_6	C_3H_8	O_2	Ar
1	298	1.42	43.1	19.51	40.73	18.62	17.07	1.58	2.48	–	–	–	–
2	49	1.32	24.1	7.74	46.69	21.34	19.57	1.82	2.84	–	–	–	–
3	155	2.50	24.1	7.74	46.69	21.34	19.57	1.82	2.84	–	–	–	–
4	45	2.50	3.3	–	–	–	–	3.56	94.58	1.66	0.20	–	–
5	138	2.50	27.4	6.76	40.78	18.64	17.09	2.04	14.46	0.21	0.03	–	–
6	610	2.00	27.4	6.76	40.78	18.64	17.09	2.04	14.46	0.21	0.03	–	–
7	1055	1.80	27.4	4.75	54.24	36.20	2.70	1.58	0.52	–	–	–	–
8	45	2.50	3.2	–	–	–	–	3.56	94.58	1.66	0.20	–	–
9	480	2.00	3.2	–	–	–	–	3.56	94.58	1.66	0.20	–	–
10	957	1.80	30.7	4.31	49.42	33.01	2.45	1.75	8.90	0.15	0.02	–	–
11	50	1.42	13.4	7.74	46.69	21.34	19.57	1.82	2.84	–	–	–	–
12	15	1.01	51.4	–	–	–	0.03	78.03	–	–	–	20.99	0.95
13	100	2.00	51.4	–	–	–	0.03	78.03	–	–	–	20.99	0.95
14	610	1.90	51.4	–	–	–	0.03	78.03	–	–	–	20.99	0.95
15	437	1.32	64.9	2.30	13.88	6.34	5.84	55.37	0.85	–	–	14.75	0.67
16	1132	1.30	64.9	19.87	–	–	14.50	61.61	–	–	–	3.28	0.74
17	40	1.10	58.9	6.18	–	–	16.97	72.14	–	–	–	3.84	0.87
18	54	1.02	47.7	13.10	–	–	1.87	79.96	–	–	–	4.25	0.82

(*continued on next page*)

Table 14 (*continued*)

Stream	Temperature [°C]	Pressure [bar]	Mass flow rate [kg/s]	Molar composition [%]									
				H_2O	H_2	CO	CO_2	N_2	CH_4	C_2H_6	C_3H_8	O_2	Ar
19	29	2.00	13.2	1.20	–	–	97.75	0.22	–	–	–	0.02	0.81
20	31	110	13.2	0.50	–	–	98.44	0.22	–	–	–	0.02	0.82
21	45	1.20	0.4	–	–	–	–	3.56	94.58	1.66	0.20	–	–
22	15	1.01	6.8	–	–	–	0.03	78.03	–	–	–	20.99	0.95
23	34	1.20	6.8	–	–	–	0.03	78.03	–	–	–	20.99	0.95
24	129	1.10	7.2	16.17	–	–	8.20	71.79	–	–	–	2.98	0.87

Table 15
Main streams specifications of the DRI-EAF+ MDEA plant.

Stream	Temperature [°C]	Pressure [bar]	Mass flow rate [kg/s]	Molar composition [%]									
				H_2O	H_2	CO	CO_2	N_2	CH_4	C_2H_6	C_3H_8	O_2	Ar
1	298	1.42	43.1	19.51	40.73	18.62	17.07	1.58	2.48	–	–	–	–
2	50	1.42	24.1	7.70	46.71	21.36	19.58	1.82	2.85	–	–	–	–
3	146	3.00	24.1	7.70	46.71	21.36	19.58	1.82	2.85	–	–	–	–
4	45	2.50	3.3	–	–	–	–	3.56	94.58	1.66	0.20	–	–
5	131	2.50	27.4	6.72	40.79	18.65	17.10	2.04	14.47	0.21	0.03	–	–
6	610	2.00	27.4	6.72	40.79	18.65	17.10	2.04	14.47	0.21	0.03	–	–
7	1055	1.80	27.4	4.73	54.24	36.23	2.69	1.58	0.53	–	–	–	–
8	45	2.50	3.2	–	–	–	–	3.56	94.58	1.66	0.20	–	–
9	480	2.00	3.2	–	–	–	–	3.56	94.58	1.66	0.20	–	–
10	957	1.80	30.7	4.31	49.42	33.01	2.45	1.75	8.90	0.15	0.02	–	–
11	50	1.42	13.4	7.70	46.71	21.36	19.58	1.82	2.85	–	–	–	–
12	287	8.00	13.4	7.70	46.71	21.36	19.58	1.82	2.85	–	–	–	–
13	318	7.25	19.4	22.92	45.49	1.67	26.69	1.26	1.97	–	–	–	–
14	40	7.15	15.1	0.91	58.48	2.14	34.31	1.62	2.54	–	–	–	–
15	55	6.00	2.9	2.28	87.22	3.10	2.03	2.41	2.96	–	–	–	–
16	20	2.00	12.4	1.20	0.07	0.19	96.91	–	1.63	–	–	–	–
17	32	110	12.3	0.50	0.07	0.19	97.60	–	1.64	–	–	–	–
18	15	1.01	51.4	–	–	–	0.03	78.03	–	–	–	20.99	0.95
19	100	2.00	51.4	–	–	–	0.03	78.03	–	–	–	20.99	0.95
20	610	1.50	51.4	–	–	–	0.03	78.03	–	–	–	20.99	0.95
21	481	2.00	54.3	0.55	21.05	0.75	0.51	59.78	0.71	–	–	15.92	0.72
22	1141	2.00	54.3	25.85	–	–	2.21	67.09	–	–	–	4.04	0.81
23	93	1.50	54.3	25.85	–	–	2.21	67.09	–	–	–	4.04	0.81
24	45	1.20	0.2	–	–	–	–	3.56	94.58	1.66	0.20	–	–
25	15	1.01	3.2	–	–	–	0.03	78.03	–	–	–	20.99	0.95
26	34	1.20	3.2	–	–	–	0.03	78.03	–	–	–	20.99	0.95
27	130	1.10	3.3	16.34	–	–	8.28	71.72	–	–	–	2.79	0.87

Table 16
Main streams specifications of the DRI-EAF+ SEWGS plant.

Stream	Temperature [°C]	Pressure [bar]	Mass flow rate [kg/s]	Molar composition [%]									
				H_2O	H_2	CO	CO_2	N_2	CH_4	C_2H_6	C_3H_8	O_2	Ar
1	298	1.42	43.1	19.51	40.73	18.62	17.07	1.58	2.48	–	–	–	–
2	49	1.32	24.1	7.74	46.69	21.34	19.57	1.82	2.84	–	–	–	–
3	155	2.50	24.1	7.74	46.69	21.34	19.57	1.82	2.84	–	–	–	–
4	45	2.50	3.3	–	–	–	–	3.56	94.58	1.66	0.20	–	–
5	138	2.50	27.4	6.76	40.78	18.64	17.09	2.04	14.46	0.21	0.03	–	–
6	610	2.00	27.4	6.76	40.78	18.64	17.09	2.04	14.46	0.21	0.03	–	–
7	1055	1.80	27.4	4.75	54.24	36.20	2.70	1.58	0.52	–	–	–	–
8	45	2.50	3.2	–	–	–	–	3.56	94.58	1.66	0.20	–	–
9	480	2.00	3.2	–	–	–	–	3.56	94.58	1.66	0.20	–	–
10	957	1.80	30.7	4.31	49.42	33.01	2.45	1.75	8.90	0.15	0.02	–	–
11	49	1.42	13.4	7.74	46.69	21.34	19.57	1.82	2.84	–	–	–	–
12	316	18.50	13.3	6.98	47.08	21.51	19.73	1.83	2.87	–	–	–	–
13	400	18.00	17.6	18.47	46.67	5.36	25.93	1.39	2.17	–	–	–	–
14	400	18.50	1.6	100	–	–	–	–	–	–	–	–	–
15	400	2.00	4.4	100	–	–	–	–	–	–	–	–	–
16	461	17.90	3.3	8.49	81.95	3.13	0.58	2.27	3.58	–	–	–	–
17	340	17.40	3.3	8.49	81.95	3.13	0.58	2.27	3.58	–	–	–	–
18	82	1.90	3.2	8.49	81.95	3.13	0.58	2.27	3.58	–	–	–	–
19	82	1.20	0.1	8.49	81.95	3.13	0.58	2.27	3.58	–	–	–	–
20	15	1.01	1.7	–	–	–	0.03	78.03	–	–	–	20.99	0.95

(*continued on next page*)

Table 16 (*continued*)

Stream	Temperature [°C]	Pressure [bar]	Mass flow rate [kg/s]	Molar composition [%]									
				H_2O	H_2	CO	CO_2	N_2	CH_4	C_2H_6	C_3H_8	O_2	Ar
21	32	1.20	1.7	–	–	–	0.03	78.03	–	–	–	20.99	0.95
22	100	1.10	1.9	28.41	–	0.06	2.10	65.49	–	–	–	3.16	0.79
23	400	1.30	20.3	60.06	0.38	0.05	39.50	0.01	–	–	–	–	–
24	147	1.20	20.3	60.06	0.38	0.05	39.50	0.01	–	–	–	–	–
25	31	110	12.6	0.65	0.95	0.12	98.25	0.03	–	–	–	–	–
26	15	1.01	49.4	–	–	–	0.03	78.03	–	–	–	20.99	0.95
27	100	2.00	49.4	–	–	–	0.03	78.03	–	–	–	20.99	0.95
28	610	1.90	49.4	–	–	–	0.03	78.03	–	–	–	20.99	0.95
29	480	1.90	52.5	2.14	20.71	0.79	0.17	58.89	0.90	–	–	15.69	0.71
30	1130	1.80	54.3	27.63	–	–	2.09	65.98	–	–	–	3.51	0.80
31	161	1.60	54.3	27.63	–	–	2.09	65.98	–	–	–	3.51	0.80
32	34	18.50	1.5	100	–	–	–	–	–	–	–	–	–
33	400	18.50	1.5	100	–	–	–	–	–	–	–	–	–
34	400	18.50	2.0	100	–	–	–	–	–	–	–	–	–
35	400	18.50	3.5	100	–	–	–	–	–	–	–	–	–
36	33	0.05	3.5	100	–	–	–	–	–	–	–	–	–
37	33	0.05	3.5	100	–	–	–	–	–	–	–	–	–
38	33	0.05	1.5	100	–	–	–	–	–	–	–	–	–
39	33	0.05	2.0	100	–	–	–	–	–	–	–	–	–

Assumptions for the modelling of MEA and MDEA carbon capture sections

The assumptions used for the modelling of the MEA post-combustion and MDEA pre-combustion carbon capture sections are shown in Table 17 and in Table 18.

Table 17
MEA and MDEA cases. Constants used in Eq. (16).

Reaction	A	B	C	D	E
$MEA^+ + H_2O \rightleftharpoons MEA + H_3O^+$	−3.038325	−7008.36	0	−0.00313489	0
$MEACCO^- + H_2O \rightleftharpoons MEA + HCO_3^-$	−0.52135	−2545.53	0	0	0
$MDEA^+ + H_2O \rightleftharpoons MDEA + H_3O^+$	−9.4165	−4234.98	0	0	0
$CO_2 + 2H_2O \rightleftharpoons H_3O^+ + HCO_3^-$	231.465	−12,092.1	−36.7816	0	0
$HCO_3^- + H_2O \rightleftharpoons H_3O^+ + CO_3^{2-}$	216.049	−12,431.7	−35.4819	0	0
$2H_2O \rightleftharpoons H_3O^+ + OH^-$	132.899	−13,445.9	−22.4773	0	0

Table 18
Assumptions adopted in the Aspen model of the MEA and MDEA carbon capture sections.

Section	Aspen Plus model	
MEA		
- Absorber	RadFraq	Equilibrium; 10 stages; Condenser: None; Reboiler: None
- Stripper	RadFraq	Equilibrium; 15 stages; Condenser: Partial-vapour-Liquid; Reboiler: Kettle
- Regenerative heat exchanger	HeatX	Pinch point $\Delta T = 10$ °C
- Pump	Pump	Discharge pressure = 3 bar; $\eta_h = 0.75$; $\eta_m = 0.95$
- CO_2 compression train	Mcompr	3 stages; Discharge pressure = 80 bar; $\eta_{p,1,2} = 0.8$; $\eta_{p,3} = 0.75$; $\eta_m = 0.95$; $T_{intercooling} = 28$ °C
	Pump	Discharge pressure = 110 bar; $\eta_h = 0.75$; $\eta_m = 0.95$
MDEA		
- Absorber	RadFraq	Equilibrium; 10 stages; Condenser: None; Reboiler: None
- Stripper	RadFraq	Equilibrium; 10 stages; Condenser: Partial-vapour-Liquid; Reboiler: Kettle
- Regenerative heat exchanger	HeatX	Pinch point $\Delta T = 10$ °C
- Pump	Pump	Discharge pressure = 7 bar; $\eta_h = 0.75$; $\eta_m = 0.95$
- CO_2 compression train	Mcompr	3 stages; Discharge pressure = 80 bar; $\eta_{p,1,2} = 0.8$; $\eta_{p,3} = 0.75$; $\eta_m = 0.95$; $T_{intercooling} = 28$ °C
	Pump	Discharge pressure = 110 bar; $\eta_h = 0.75$; $\eta_m = 0.95$

Assumptions for the techno-economic analysis

The assumptions for the techno-economic analysis (Table 19 and 21) as well as the reference costs of the equipment (Table 20) are shown in this section.

Table 19
Assumptions for the techno-economic analysis.

Parameter	Unit	Value
DRI-EAF CAPEX	[€/t_{HRC}]	87
DRI-EAF fixed OPEX	[€/t_{HRC}]	80
CAPEX increase for H_2 fired reformer	[% DRI-EAF CAPEX]	5
Fixed O&M increase for CO_2 capture section	[% $TPC_{CC\ section}$]	5
Iron ores price	[€/t_{HRC}]	74
Natural gas price	[€/GJ (LHV)]	20
Electricity price	[€/MWh]	150
CO_2 transport and storage	[€/t_{CO2}]	20
CO_2 tax	[€/t_{CO2}]	0
MEA price	[€/kg]	1.25
MDEA price	[€/kg]	1.25
Raw water price	[€/t]	1
Natural gas boiler efficiency	[%]	92
Plants availability	[h/y]	8200
Plants lifetime	[years]	25
Interest rate	[%]	11
Fixed charge factor	[%]	11.87
ton_{DRI}/ton_{HRC}	[-]	1.2

Table 20
Equipment reference costs.

Component	Scaling parameter	C_0 [M€]	S_0	f	Ref.
CO_2 capture unit (MEA)	CO_2 mass flow rate, kg/s	28.95	38.4	0.8	(Anantharaman et al., 2011)
CO_2 capture unit (MDEA)	CO_2 mass flow rate, t/h	8.8	12.4	0.6	(Khallaghi et al., 2022)
CO_2 compressor and condenser	Power, MW	9.95	13	0.67	(Anantharaman et al., 2011)
Compressor	Power, MW	8.1	15.3	0.67	(Khallaghi et al., 2022)
Boiler	Heat duty, MW	0.25	1	0.67	(Khallaghi et al., 2022)
Pump	Volumetric flow, m^3/h	0.017	250	0.14	(Khallaghi et al., 2022)
Heat exchanger	Heat transfer, MW	6.1	828	0.67	(Khallaghi et al., 2022)
WGS	H_2 and CO flow rate, kmol/s	18.34	2.45	0.65	(Khallaghi et al., 2022)
SEWGS single train	Inlet mole flow rate, kmol/s	8.88	1.56	0.67	(Manzolini et al., 2020)
Gas turbine	Power [MW]	49.4	272.1	0.67	(Khallaghi et al., 2022)
Fuel Compressor	Power [MW]	8.1	15.3	0.67	(Khallaghi et al., 2022)
Steam turbine	Power [MW]	33	200	0.67	(Khallaghi et al., 2022)
HRSG	U•S [MW/K]	32.6	12.9	0.67	(Khallaghi et al., 2022)
Condenser	Heat transfer [MW]	6.1	828	0.67	(Khallaghi et al., 2022)
Cooling tower	Heat rejected [MW]	49.6	470	0.67	(Khallaghi et al., 2022)

Table 21
Methodology used to compute the total plant cost of the additional equipment (Manzolini et al., 2020).

Cost		Power generation section	CO_2 capture section
Total Installation Cost	[% TEC]	66	104
Indirect Costs	[% (TEC+TIC)]	14	14
Contingency	[% (TEC+TIC+IC)]	10	10
Owner's Cost	[% (TEC+TIC+IC)]	5	5

Reference BF-BOF plant

The DRI-EAF plants presented in this work are compared to a reference BF-BOF steel mill. The plant size is 3.16 Mt_{HRC}/y corresponding to a coal consumption equal to 6240 t/d. The simplified block flow diagram is shown in Fig. 14. The three residual steel gases, namely the blast furnace gas (BFG), the basic oxygen gas (BOFG) and the coke oven gas (COG), are used to provide 682 MW_{th} and 159 MW_e. The electricity necessary to run the steel plant is generated in a combined cycle having an efficiency of 52% where BFG and BOFG are used as fuels (Table 22, Fig. 14).

The main raw materials in a BF-BOF plant are coal, iron ores, and lime. Coal is used as an energy agent as well as a reducing and carburization agent. In the coke plant, coal is converted to coke releasing the coke oven gas. The so called "underfired heating" process provides the energy to the coke ovens, using part of the COG and of the BFG as energy sources. Lime is produced heating calcium carbonate to high temperatures. Coke, lime and iron ores are agglomerated in the sintering plant. COG provides the energy required by the lime and the sintering production steps. The sintered agglomerates, with coke and other additives are injected at the top of the blast furnace. In the blast furnace iron ores are reduced to iron. In addition, a hot blast and pulverised coal are fed into the blast furnace. A hot liquid metal leaves the blast furnace bottom while BFG is generated as by-product. Iron is then converted into steel in the basic oxygen furnace where the carbon content is reduced from approximately 4% to less than 1.5% by oxygen addition. Basic oxygen furnace gas is produced here. In the last steps iron is converted into the final steel products.

The specific CO_2 emissions generated by the combustion of the residual steel gases are listed in Table. 22. In addition, also the emissions related to

the iron ore production are taken into account. They are computed according to the carbon intensity of the grid electricity as indicated in Table 2.

Table 22
BFG, BOFG and COG mass flow rate and composition.

Stream	Mass flow rate [kg/s]	Power (LHV) [MW]	Emissions [t_{CO2}/t_{HRC}]	Mass composition [%]								
				H_2	N_2	O_2	CO	CO_2	Ar	H_2O	CH_4	HHC
BFG (internal use)	160.9	366	0.947	2.4	53.5	0.0	22.7	21.4	0.0	0.0	0.0	0.0
BFG (power plant)	125.1	285	0.736	2.4	53.5	0.0	22.7	21.4	0.0	0.0	0.0	0.0
BOFG (internal use)	13.3	73	0.138	3.3	18.8	0.0	56.4	20.8	0.6	0.0	0.0	0.0
BOFG (power plant)	4.4	24	0.045	3.3	18.8	0.0	56.4	20.8	0.6	0.0	0.0	0.0
COG (internal use)	7.3	286	0.107	59.5	5.8	0.2	3.8	1.0	0.0	4.0	23.0	2.7

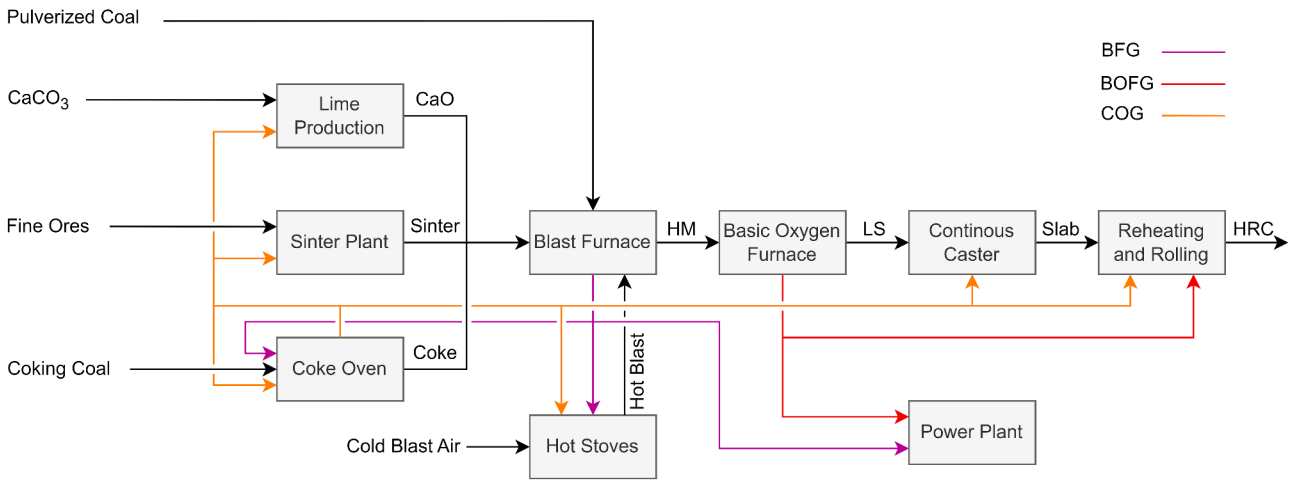

Fig. 14. BF-BOF plant block flow diagram.

References

Alamsari, B., Torii, S., Trianto, A., Bindar, Y., 2011. Heat and mass transfer in reduction zone of sponge iron reactor. ISRN Mech. Eng. 324659 https://doi.org/10.5402/2011/324659.

Alamsari, B., Torii, S., Trianto, A., Bindar, Y., 2010. Study of the effect of reduced iron temperature rising on total carbon formation in iron reactor isobaric and cooling zone. Adv. Mechan. Eng. 2, 192430 https://doi.org/10.1155/2010/192430.

Alhumaizi, K., Ajbar, A., Soliman, M., 2012. Modelling the complex interactions between reformer and reduction furnace in a midrex-based iron plant. Can. J. Chem. Eng. 90, 1120–1141. https://doi.org/10.1002/cjce.20596.

Anantharaman, R., Bolland, O., Booth, N., van Dorst, E., Ekstrom, C., Sanchez Fernandez, E., Franco, F., Macchi, E., Manzolini, G., Nikolic, D., Pfeffer, A., Prins, M., Rezvani, S., Robinson, L., 2011. CAESAR: carbon-free electricity by SEWGS: advanced materials, reactor, and process design. Collaborative large-scale integrating project - European best practice guidelines for assessment of CO2 capture technologies.

Béchara, R., Hamadeh, H., Mirgaux, O., Patisson, F., 2018. Optimization of the iron ore direct reduction process through multiscale process modeling. Materials (Basel) 11. https://doi.org/10.3390/ma11071094.

Boon, J., Cobden, P.D., van Dijk, H.A.J., Hoogland, C., van Selow, E.R., van Sint Annaland, M., 2014. Isotherm model for high-temperature, high-pressure adsorption of CO2 and H2O on K-promoted hydrotalcite. Chem. Eng. J. 248, 406–414. https://doi.org/10.1016/J.CEJ.2014.03.056.

Boon, J., Cobden, P.D., van Dijk, H.A.J., van Sint Annaland, M., 2015. High-temperature pressure swing adsorption cycle design for sorption-enhanced water–gas shift. Chem. Eng. Sci. 122, 219–231. https://doi.org/10.1016/J.CES.2014.09.034.

Boon, J., Coenen, K., van Dijk, E., Cobden, P., Gallucci, F., van Sint Annaland, M., 2017. Sorption-enhanced water–gas shift. Adv. Chem. Eng. 51, 1–96. https://doi.org/10.1016/bs.ache.2017.07.004.

Cavaliere, P., 2019. Clean Ironmaking and Steelmaking Processes, Clean Ironmaking and Steelmaking Processes. Springer International Publishing. https://doi.org/10.1007/978-3-030-21209-4.

Demus, T., Echterhof, T., Pfeifer, H., Schulten, M., 2012. Investigation of the use of biogenic residues as a substitute for fossil coal in the EAF steelmaking process.

Duarte, P., Scarnati, T., Becerra, J., 2008. ENERGIRON direct reduction technology - economical, flexible, environmentally friendly.

Gentile, G., Bonalumi, D., Pieterse, J.A.Z., Sebastiani, F., Lucking, L., Manzolini, G., 2022. Techno-economic assessment of the FReSMe technology for CO2 emissions mitigation and methanol production from steel plants. J. CO2 Util. 56 https://doi.org/10.1016/j.jcou.2021.101852.

Hamadeh, H., Mirgaux, O., Patisson, F., 2018. Detailed modeling of the direct reduction of iron ore in a shaft furnace. Materials (Basel) 11. https://doi.org/10.3390/ma11101865.

Hou, B., Zhang, H., Li, H., Qingshan, Z., 2012. Study on kinetics of iron oxide reduction by hydrogen. Chin. J. Chem. Eng. https://ec.europa.eu/eurostat.

International Energy Agency, 2020. Iron and steel technology roadmap towards more sustainable steelmaking part of the energy technology perspectives series.

Jansen, D., Gazzani, M., Manzolini, G., Dijk, E.van, Carbo, M., 2015. Pre-combustion CO2 capture. Int. J. Greenhouse Gas Control 40, 167–187. https://doi.org/10.1016/j.ijggc.2015.05.028.

Khallaghi, N., Abbas, S.Z., Manzolini, G., De Coninck, E., Spallina, V., 2022. Techno-economic assessment of blast furnace gas pre-combustion decarbonisation integrated with the power generation. Energy Convers. Manag. 255 https://doi.org/10.1016/j.enconman.2022.115252.

Kirschen, M., Badr, K., Pfeifer, H., 2011. Influence of direct reduced iron on the energy balance of the electric arc furnace in steel industry. Energy 36, 6146–6155. https://doi.org/10.1016/j.energy.2011.07.050.

Lu, F., Wen, L., Zhao, Y., Zhong, H., Xu, J., Zhang, S., Yang, Z., 2019. The competitive adsorption behavior of CO and H2 molecules on FeO surface in the reduction process. Int. J. Hydrogen Energy 44, 6427–6436. https://doi.org/10.1016/J.IJHYDENE.2019.01.173.

Manzolini, G., Giuffrida, A., Cobden, P.D., van Dijk, H.A.J., Ruggeri, F., Consonni, F., 2020. Techno-economic assessment of SEWGS technology when applied to integrated steel-plant for CO2 emission mitigation. Int. J. Greenhouse Gas Control 94. https://doi.org/10.1016/j.ijggc.2019.102935.

Muscolino, F., Martinis, A., Ghiglione, M., Duarte, P., 2016. Introduction to direct reduction technology and outlook for its use. La Metallurgia Italiana - n 4, 25–31.

Nouri, S.M.M., Ale Ebrahim, H., Jamshidi, E., 2011. Simulation of direct reduction reactor by the grain model. Chem. Eng. J. 166, 704–709. https://doi.org/10.1016/J.CEJ.2010.11.025.

Palacios, P., Toledo, M., Cabrera, M., 2015. Iron ore reduction by methane partial oxidation in a porous media. Int. J. Hydrogen Energy 40, 9621–9633. https://doi.org/10.1016/J.IJHYDENE.2015.05.058.

Parisi, D.R., Laborde, M.A., 2004. Modeling of counter current moving bed gas-solid reactor used in direct reduction of iron ore. Chem. Eng. J. 104, 35–43. https://doi.org/10.1016/j.cej.2004.08.001.

Rahimi, A., Niksiar, A., 2013. A general model for moving-bed reactors with multiple chemical reactions part I: model formulation. Int. J. Miner. Process. 124, 58–66. https://doi.org/10.1016/J.MINPRO.2013.02.015.

Ranzani da Costa, A., Wagner, D., Patisson, F., 2013. Modelling a new, low CO2 emissions, hydrogen steelmaking process. J. Clean Prod. 46, 27–35. https://doi.org/10.1016/j.jclepro.2012.07.045.

Rechberger, K., Spanlang, A., Sasiain Conde, A., Wolfmeir, H., Harris, C., 2020. Green hydrogen-based direct reduction for low-carbon steelmaking. Steel Res. Int. 91 https://doi.org/10.1002/srin.202000110.

Remus, R., Aguado-Monsonet, M.A., Roudier, S., Delgado Sancho, L., 2013. Best available techniques (bat) reference document for iron and steel production - industrial emissions directive 2010/75/eu (integrated pollution prevention and control).

Sarkar, S., Bhattacharya, R., Roy, G.G., Sen, P.K., 2018. Modeling MIDREX based process configurations for energy and emission analysis. Steel Res. Int. 89 https://doi.org/10.1002/srin.201700248.

Shams, A., Moazeni, F., 2015. Modeling and simulation of the MIDREX shaft furnace: reduction, transition and cooling zones. JOM 67, 2681–2689. https://doi.org/10.1007/s11837-015-1588-0.

Vogl, V., Åhman, M., Nilsson, L.J., 2018. Assessment of hydrogen direct reduction for fossil-free steelmaking. J. Clean Prod. 203, 736–745. https://doi.org/10.1016/j.jclepro.2018.08.279.

Weiss, B., Sturn, J., Voglsam, S., Winter, F., Schenk, J., 2011. Industrial fluidised bed direct reduction kinetics of hematite ore fines in H2 rich gases at elevated pressure. Chem. Eng. Sci. 66, 703–708. https://doi.org/10.1016/j.ces.2010.11.024.

World direct reduction statistics, 2020.

Zare Ghadi, A., Valipour, M.S., Biglari, M., 2017. CFD simulation of two-phase gas-particle flow in the Midrex shaft furnace: the effect of twin gas injection system on the performance of the reactor. Int. J. Hydrogen Energy 42, 103–118. https://doi.org/10.1016/J.IJHYDENE.2016.11.053.